Chemical Engineering Journal 477 (2023) 147239

Contents lists available at ScienceDirect

Chemical Engineering Journal

journal homepage: www.elsevier.com/locate/cej

Euler-Euler LES of bubble column bubbly flows by considering sub-grid scale turbulent dispersion effect on modulating bubble transport

Shanshan Long [a], Xiaogang Yang [a,*], Jie Yang [b], Bin Li [a], Weibin Shi [c], Martin Sommerfeld [d]

[a] Department of Mechanical, Materials and Manufacturing Engineering, University of Nottingham Ningbo China, University Park, Ningbo 315100, PR China
[b] School of Natural Sciences, University of Hull, Hull HU6 7RX, UK
[c] College of Mechanical Engineering and Automation, Huaqiao University, Xiamen 361021, Fujian Province, PR China
[d] Multiphase Flow Systems, Institute for Process Engineering, Otto-von-Guericke-University Magdeburg, Hoher Weg 7b, D-06120 Halle (Saale), Germany

ARTICLE INFO

Keywords:
LES simulation
Turbulent dispersion
Bubble oscillation
Bubble Column

ABSTRACT

It has now been recognised and generally accepted that turbulent dispersion may be modelled using the time average of the fluctuating part of the interphase momentum, employing the drag the Favre averaged drag model for turbulent dispersion in Eulerian multi-phase flows. As the turbulent eddies in the surrounding of bubbles interact strongly with the bubbles in bubbly flow, the bubble trajectories and bubble oscillation take place accordingly as the consequence of continuous deformation of the bubble surfaces. When using large eddy simulation for modelling bubbly flow, the sub-grid scale (SGS) filtered velocity fluctuations of liquid phase can be interpreted as many small eddies that may act on the surface of bubbles, consequently giving rise to bubble shape variations and the dispersion of bubbles. This study employs Euler/Euler large-eddy simulation (LES) modelling to demonstrate that the turbulent dispersion force model can be used to effectively indicate the influence of turbulent eddies on bubble dynamics, in particular the bubble cluster oscillations, which leads to remarkable improvements in the prediction of bubble lateral dispersion behaviour. The use of spatial filtering to model the SGS bubble dispersion is proposed with a modification on SGS eddy viscosity to reflect turbulent dispersion due to bubble induced turbulence. The results of the time-averaged LES modelled bubble velocities and bubble volume fraction profiles are in good agreement with the experimental data while the turbulent kinetic energy spectrum obtained at different locations on the centreline of the bubble column still exhibits the conventional −5/3 scaling for shear induced turbulence and a −3 scaling for bubble induced turbulence.

1. Introduction

When employing the Euler-Euler large eddy simulation (LES) approach in the prediction of bubble column bubbly flows, modelling of the interfacial interactions between the bubbles and carrier fluid plays a key role in evaluation of the hydrodynamics, in particular shear turbulence and bubble induced turbulence characteristics, and heat and mass transfer. Recent progress on modelling the interphase forces involved in bubble column bubbly flows has led to several versions of modified models for interfacial force closure, in particular for the drag force experienced by the bubbles. However, there is still no consensus formed so far for contributions from each individual interfacial force considered in modelling bubble column bubbly flows. Representative cases are: i) neglecting the contribution of transverse lift forces [32,30,5,19,38]; ii) ignoring the effect of virtual mass force [42,44,18,10,39]; iii) negligible contribution of wall lubrication force compared with other interfacial forces [37]) and considering wall lubrication force with three typical models [1], Tomiyama, 1995, [16]. However, the results using these different models have revealed the effect on the prediction not to be notable; iv) disregarding the turbulent dispersion force (TDF), especially in RANS modelling [31,6,13,23,15], Burns *et al.*, 2004, [22].

Of particular concern in this work is the importance of turbulent dispersion in modulating the bubble transportation in bubble column bubbly flows. Formulation of the mechanisms behind the contribution of turbulent dispersion remains challengeable since the derivation of the two-phase flow governing equations may employ different averaging approaches. However, characterisation of the effect of turbulent dispersion on bubble transport in terms of turbulent dispersion force can provide certain insights into its interactions with surrounding eddies. When using the turbulent dispersion force to describe the eddy diffusion effect, the bubble volume fraction gradient is needed to calculate the

* Corresponding author.
E-mail address: Xiaogang.Yang@nottingham.edu.cn (X. Yang).

https://doi.org/10.1016/j.cej.2023.147239
Received 9 March 2023; Received in revised form 2 November 2023; Accepted 7 November 2023
Available online 9 November 2023

Nomenclature

A [m^{-1}]	Area density
a [m^2]	Interfacial area per unit volume
C_D[-]	Drag coefficient
C_{TD}[-]	Turbulent dispersion coefficient
C_L[-]	Lift coefficient
C_{AM}[-]	Added mass coefficient
$\overline{D}$[m^2/s]	Mass diffusivity
d[m]	Bubble diameter
E_0[-]	Eötvös number
f [Hz]	Frequency
$\mathbf{M}_D$[N/m^3]	Drag force
$\mathbf{M}_L$[N/m^3	Lift force
$\mathbf{M}_{AM}$[N/m^3]	Added mass force
$\mathbf{M}_{TD}$[N/m^3]	Turbulent dispersion force
g[m/s^2]	Gravity acceleration
K_L[m/s]	Convective mass transfer film coefficient
Q [s^{-2}]	Invariant Q-criterion
Re[-]	Reynolds number
Sh[-]	Sherwood number
Sc[-]	Schmidt number
u[m/s]	Velocity vector
ω[s^{-1}]	Water vorticity

Greek letters

α[-]	Phase volume fraction, gas holdup
ε[m^2/s^3]	Turbulence dissipation rate
λ[m]	Characteristic length scale of eddy
μ[Pa • s]	Liquid dynamic viscosity
μ_{eff}[Pa • s]	Effective viscosity of the liquid phase
Δ[m]	LES delta
κ[m^{-1}]	Wave number
γ [-]	Volume increment ratio

Subscripts

B	Bubble
G	Gas phase
L	Liquid phase
max	Maximum
SGS	Sub-grid scale

gas-phase flux in the mass conservation equation. The shortcoming of using this modelled force is that it may still give out the unrealistic result of existence of the dispersed phase flux even when the dispersed phase velocity is zero. As a result, the bubble dispersion cannot be indicated using the continuity equation when employing Favre averaging formulation instead such effect is reflected as a source term in the momentum equation [43]. Generally speaking, the turbulent dispersion can be modelled in the following means: (i) being proportional to the volume fraction gradient [21,4], Drew, 2001); (ii) being proportional to the product of the gradient of bubble volume fraction and the liquid turbulent kinetic energy (de Bertodano, 1992, [21]; (iii) being proportional to the Reynolds stress tensor (Drew, 2001, de Bertodano, 1998); (iv) a proposed random dispersion model without any tuneable coefficients [11] and (v) a Favre-Averaged Drag (FAD) model by conducting the double-time averaging of drag term in the Reynolds time-averaged momentum transport equation for multiphase flows in the Eulerian frame (Burns *et al.*, 2004). Burns' *et al.* model has been mathematically analysed and validated for modelling turbulent dispersion. Additionally, their FAD turbulent dispersion force model can still perform well in many CFD simulations for bubbly flows even if the appropriate value of turbulent dispersion coefficient, $C_{TD,}$ is not used. As pointed out by Lavieville *et al.* (2017), such turbulent dispersion may result in the bubbles dispersing from the high concentration region to the low concentration region, and consequently make the local bubble volume fraction peak smooth in the bubbly flows. The turbulent dispersion force has been also discussed and the formulation has been proposed by Lubchenko et al. [26], again assuming the hypothesis of the dispersion associated with the gradient of local bubble volume fraction. Lahey *et al.* (1993) conducted both experiments and numerical simulations to analyse the lateral phase distribution of the gas–liquid two-phase flow. In their CFD modelling, the turbulent dispersion force proposed by de Bertodano was employed but the proportionality coefficient C_{TD} was set to 0.1. Drew (2001) proposed a relationship for describing turbulent dispersion, which is suitable for bubbly flows mainly to account for the ratio of turbulent eddy time scale to bubble relaxation time scale, i.e., the reciprocal of the Stokes number. Lucas et al. [27] have indicated that the extra turbulence dispersion force caused by bubble deformation induced turbulence is necessary for predicting the radial bubble volume fraction distribution in the pipe bubbly flows. They indicated that the bubble deformation induced turbulence may play a role in smoothing the radial bubble volume fraction profiles in gas–liquid two-phase bubbly flow in the pipe.

As turbulent eddies interact with the bubbles in bubbly flows, the prediction of turbulence dispersion needs a suitable turbulence model and reasonable near-wall treatment while such models are usually associated with the turbulent eddy viscosity and turbulent intensity. For turbulent eddies with scales within the range of inertial sub-range (where Taylor integral length scale usually is located in this range) and larger than the imposed grid size, the use of large eddy simulation (LES) modelling can be a suitable alternative to resolve the turbulent dispersion effect for larger scales. The spatial turbulent eddy fluctuations can be partially recognised in the LES spatial filtering process. Consequently, the impact of the SGS eddy fluctuation on bubble dispersion can be modelled. In addition, the shear turbulence generated in the liquid phase significantly affects the entrainment and migration of bubbles because bubbles may be entrapped by larger eddies while they may also be bombarded by turbulent eddies with sizes smaller than the bubbles [2]. The turbulent dispersion force model proposed by de Bertodano (1994) was able to describe the influence of liquid phase turbulent kinetic energy with the local turbulent intensity on the discrete phase (bubbles) dispersion in the bubbly flow. The model proposed by Burns *et al.* (2004) also considered the effects of turbulent eddy viscosity and turbulent Prandtl number on the dispersion characteristics of the dispersed phase. Lavieville *et al.* (2017) attempted to propose a generalised turbulent dispersion (GTD) model based on the assumption that the influence of liquid turbulence on the drag force is dominant in bubbly flow but the model also considered the additional terms as the result of the statistical average of drag coefficient C_D and mass coefficient C_{VM}. The aforementioned work were based on the RANS modelling approach. Tabib and Schwarz [43] proposed a sub-grid-scale turbulent dispersion force model for large eddy simulation (LES) by introducing the SGS turbulent kinetic energy to replace those fluctuation velocities in de Bertodano's model.

It should be further mentioned that as the turbulent eddies strongly interact with the bubbles, the surface of bubbles are continuously hit by the eddies, which would cause the bubble deformation. As a result, the mass centres of bubbles would oscillate. Phenomenally, one can observe the bubbles to tumble in the bubble column. Sommerfeld et al. [41] adopted LES-Eulerian-Lagrangian modelling to study bubble dynamics with focus on bubble oscillations and tumbling motion in the bubble column using the bubble motion equation that accounts for drag, transverse lift, added mass, and wall forces. Their work have also

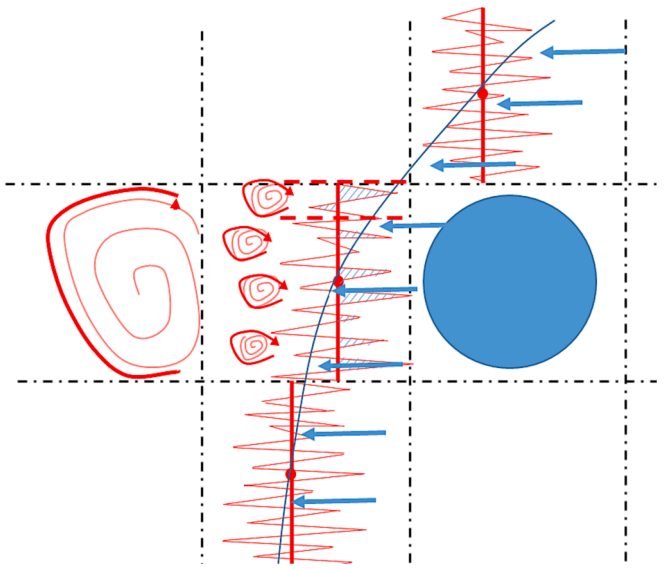

Fig. 1. Schematic of turbulent eddy fluctuations around the bubbles using the LES spatial filtering in bubble column bubbly flows. The zigzag lines indicate the filtered fluctuation of velocities of liquid phase. A hat-like filtering (box function) was adopted.

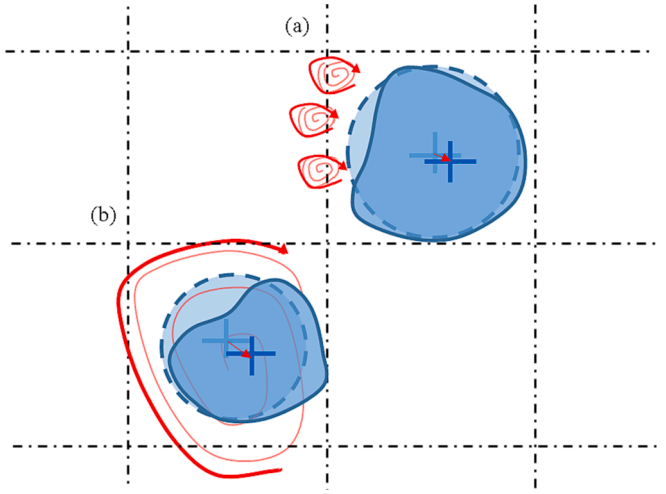

Fig. 2. Bubble shape variation caused by smaller turbulent eddies hitting on the surface of the bubbles and larger turbulent eddies trapping the bubbles with the size being smaller than the eddies and the applied shear on the bubbles causing the bubble deformation.

implemented the sub-grid-scale-turbulence modulation in the LES simulation [31]and demonstrated such SGS turbulence modulation may have the significant effect on bubble wriggling in its trajectory. As the turbulence dispersion plays a role in redistributing the bubble volume fraction in the bubble column, it can be expected that the turbulent dispersion would have the impact on bubble dynamics in the bubble column.

When employing the Eulerian-Eulerian modelling approach to model bubbly flow, the averaging procedure will normally give rise to the so-called turbulent dispersion force term in the interphase momentum exchange source terms. The turbulent dispersion force can be regarded as a hydrodynamic interaction that the carrier phase turbulent eddies entrain the bubbles, consequently contributing to the change in the radial spreading of bubble volume fraction profile [29]. In order to mimic the bubble dynamics such as bubble cluster fluctuation using the frame of Eulerian-Eulerian modelling approach, one may interpret the bubble tumbling and deformation as the consequence of the interactions between bubbles and the surrounding turbulent eddies. Here, the turbulent fluctuations can be envisaged as the different size of small eddies continuously acting on the surfaces of the bubbles. In reality, the reason for this tumbling motion can be described by the observation of clustered bubble oscillation. The turbulent fluctuations caused by turbulent eddies due to LES filtering process can be interpreted as a number of adjacent and anisotropic small eddies acting on the bubbles as illustrated in Fig. 1. The surficial shapes of the bubbles dynamically deform as the consequence of the continuous hitting by these surrounding eddies, which will either stretch or squeeze the large bubble simultaneously as schematically illustrated in Fig. 2(a) and (b). As a result, this action may lead to the fluctuation of the bubble mass-centre. The bubbles may also be entrapped in a relatively larger eddy and deformed by the eddy induced shear. These may eventually contribute to the oscillation of the bubble mass centre as can be schematically indicated in Fig. 2. Thus, the interphase forces exerting on the dispersed phase are strongly affected by interactions between the bubbles and the shear caused by nearby turbulent eddies. These interfacial momentum transfer exchanges have to be properly implemented in the sub-grid scale LES modelling for bubble column bubbly flows. While the contribution of the turbulent dispersion has been overlooked by some previous studies related to the bubble dynamics, it becomes necessary to highlight the impact of turbulent dispersion force on bubble fluctuations in the coupled SGS Eulerian-Eulerian LES modelling. In other words, the effort of the modification of turbulent dispersion force on bubble dynamics can be viewed in the frame of the sub-grid scale. As it has been widely recognised that the use of Eulerian-Eulerian two-fluid model approach can efficiently describe both carrier and dispersed phase dynamics with lower computational demand, especially for large-scale systems, the aim of the present work will further elucidate the effect of considering turbulent dispersion force on the bubble dynamics in the bubble column.

In the present study, we examine the effect of adopting the spatial filtering to the interfacial momentum exchange term on the turbulent dispersion of bubbles in bubble column bubbly flows, with reference to the drag force acting on the bubbles and its proportionality to the slip velocity between the phases and interfacial area density. By taking both phase velocity fluctuations and interfacial area density fluctuations into account, the spatial filtering of the drag force term will give rise to an extra term proportional to the area density slip velocity correlation i.e., turbulent dispersion. After employing the SGS eddy diffusivity hypothesis, the spatial-filtered drag force term is used to mimic the turbulent dispersion effect in the frame of Eulerian-Eulerian two-fluid model approach, implicitly revealing the dynamic behaviour of bubble tumbling in the bubble column. The modified SGS eddy viscosity ν_T will be also implemented into the filtered turbulent dispersion term in the modified SGS Smagorinsky model, taking into consideration the bubble dynamic response to the eddy induced shear [25]. The paper is organised as follows. The essential mathematical modelling and the numerical method for bubble column bubbly flow are described in Section 2. In Section 3, we summarise the numerical results, considering the effect of turbulent dispersion on bubble entrainment by turbulent eddies. Discussions on the various statistics involving the fluctuating velocity field, and turbulent kinetic energy spectra, with prominence given to the large-scale structure of bubble transport in the bubble column, are presented. Implications for turbulent dispersion that may partially play a role in giving rise to bubble cluster oscillation and flucuation in the bubble column are also given. The main conclusions are presented in Section 4.

2. Mathematical modelling and numerical methods

2.1. Mathematical modelling

The two-fluid model is employed based on the LES spatial filtering of mass and momentum conservation equations. In the current work, both

Table 1
Interphase force closure adopted in the LES modelling.

Forces	Expressions
Drag	$\mathbf{M}_{\mathrm{D,L}} = \frac{3}{4}\alpha_{\mathrm{G}}\rho_{\mathrm{L}}\frac{\mathrm{C_D}}{\mathrm{d_B}}\lvert\mathbf{u_G}-\mathbf{u_L}\rvert(\mathbf{u_G}-\mathbf{u_L}),\ \mathrm{C_D} = \frac{2}{3}\mathrm{E_O^2},\ \mathrm{Eo} = \frac{\mathrm{g}\Delta\rho\mathrm{d_B^2}}{\sigma}$
Lift (Tomiyama, 1998)	$\mathbf{M}_{\mathrm{L,L}} = \rho_{\mathrm{L}}\mathrm{C_L}(\mathbf{u_B}-\mathbf{u_L})\times(\nabla\times\mathbf{u_L}),\ \mathrm{C_L} = \begin{cases}\min[0.288\tanh(0.121\mathrm{Re_B}),\mathrm{f(Eo)}\ ] & \mathrm{Eo}\le 4\\ \mathrm{f(Eo)} & 4<\mathrm{Eo}<10\\ -0.29 & \mathrm{Eo}>10\end{cases}$ $\mathrm{f(Eo)} = 0.00105\mathrm{Eo}^3-0.0159\mathrm{Eo}^2-0.0204\mathrm{Eo}+0.474$ $\mathrm{d_h} = \mathrm{d}\left(1+0.163\mathrm{Eo}^{0.757}\right)^{1/3}$
Added mass	$\mathbf{M}_{\mathrm{AM,L}} = \alpha_{\mathrm{G}}\rho_{\mathrm{L}}\mathrm{C_{AM}}\left(\frac{\mathrm{D}\mathbf{u_G}}{\mathrm{D}t}-\frac{\mathrm{D}\mathbf{u_L}}{\mathrm{D}t}\right)$

the continuous liquid phase and dispersed bubble phase are modelled as two interpenetrating continuums. When employing the Eulerian-Eulerian two-fluid model, each phase requires separate filtered equations. In this LES modelling, the superimposed fluctuations $\widetilde{\phi}_k = \phi_k + \phi_k^{'}$ represent the portion of flow details evolving in the filter width Δ that have been smoothed out but this also includes the possible bubble-induced fluctuations. Here $\widetilde{\phi}_k$ is the instantaneous parameter and $\phi_k^{'}$ stands for the sub-grid scale (SGS) parameter, which needs to be modelled. It should be noted that the filter width Δ should strictly be larger than the length scale characteristic of the dispersed phase; e.g. the bubble diameter. The governing equations used in this work have been summarized in the appendix. The filtered momentum exchange term can thus be classified as different contributions from the interface forces, which are defined by

$$\boldsymbol{M}_{F,L} = -\boldsymbol{M}_{F,G} = \boldsymbol{M}_{D,L} + \boldsymbol{M}_{L,L} + \boldsymbol{M}_{VM,L} + \boldsymbol{M}_{TD,L} \tag{1}$$

The adopted forces expressions are summarised in Table 1.

With regards to the turbulent dispersion term $\boldsymbol{M}_{TD,L}$, it can be obtained by spatial filtering the phase-averaged interface drag force term. The mechanism responsible for bubble acceleration due to liquid phase velocity fluctuations is associated with the interphase momentum transfer. Thus, it would be reasonable to assume that turbulent dispersion can be modelled by using the spatial filtering of the fluctuating part of the interphase momentum force, especially the drag force. We restrict our attention here to the interphase drag force. The interphase drag force can then be specified to be proportional to slip velocity and area density,

$$\widetilde{\boldsymbol{M}}_D = \frac{1}{8}\widetilde{C}_D\widetilde{A}_{GL}\rho_G\left|\widetilde{\boldsymbol{u}}_G-\widetilde{\boldsymbol{u}}_L\right|\left(\widetilde{\boldsymbol{u}}_G-\widetilde{\boldsymbol{u}}_L\right) \tag{2}$$

where the bubble area density is given by

$$\widetilde{A}_{GL} = 6\frac{\widetilde{\alpha}_G}{d_B}. \tag{3}$$

Taking the spatial filtering of Eq. (3) by accounting for velocity fluctuations and area density fluctuations, Eq. (4) is obtained,

$$\begin{aligned}\boldsymbol{M}_D &= \boldsymbol{M}_{D,L} + \boldsymbol{M}_{TD,L}\\ &= \frac{1}{8}C_D A_{GL}\rho_G|\boldsymbol{u}_G-\boldsymbol{u}_L|(\boldsymbol{u}_G-\boldsymbol{u}_L) + \frac{1}{8}C_D\rho_G|\boldsymbol{u}_G-\boldsymbol{u}_L|\overline{A_{GL}^{'}(\boldsymbol{u}_G^{'}-\boldsymbol{u}_L^{'})}\end{aligned} \tag{4}$$

where the drag coefficient and bubble diameter have been assumed to remain unchanged in the spatial filtering process. It can be seen from Eq. (4) that the filtering of the interfacial drag force gives rise to the filtered drag term, written in terms of spatial-filtered variables, plus an extra term proportional to the area density-slip-velocity correlation $\frac{1}{8}C_D\rho_G|\boldsymbol{u}_G-\boldsymbol{u}_L|\overline{A_{GL}^{'}(\boldsymbol{u}_G^{'}-\boldsymbol{u}_L^{'})}$. If this correlation is modelled by using the SGS eddy diffusivity hypothesis, this is given by

$$\frac{1}{8}C_D\rho_G|\boldsymbol{u}_G-\boldsymbol{u}_L|\overline{A_{GL}^{'}(\boldsymbol{u}_G^{'}-\boldsymbol{u}_L^{'})} = \frac{1}{8}C_D\rho_G|\boldsymbol{u}_G-\boldsymbol{u}_L|\left(\frac{\nu_{SGS,G}}{\sigma_{SGS,G}}-\frac{\nu_{SGS,L}}{\sigma_{SGS,L}}\right)\frac{\nabla\overline{A_{GL}}}{\overline{A_{GL}}} \tag{5}$$

where $\overline{A_k^{'}\boldsymbol{u}_k^{'}}$ is related to turbulent dispersion as it reflects the effect of turbulent eddies interaction with bubbles on the change of bubble interfacial area, caused by turbulent eddy fluctuations characterised by the fluctuating velocities. By analogy with the eddy diffusivity hypothesis, the relationship between the SGS area density fluctuation and SGS relative velocities can be specified in the format of relationship between volume fraction and fluctuation velocity and modelled with aid of Eq. (4), which is given by

$$\frac{\overline{A_{GL}^{'}(\boldsymbol{u}_G^{'}-\boldsymbol{u}_L^{'})}}{\overline{A_{GL}}} = \frac{\overline{\alpha_G^{'}(\boldsymbol{u}_G^{'}-\boldsymbol{u}_L^{'})}}{\overline{\alpha_G}} \tag{6}$$

where $\nu_{SGS,k}$ is the SGS turbulent kinematic viscosity and $\sigma_{SGS,L}$ denotes the SGS turbulent Schmidt number in terms of the interfacial area density. $\sigma_{SGS,L} = 0.9$ has been used in the present study. Thus, the turbulent dispersion term can be expressed and simplified as

$$\begin{aligned}\boldsymbol{M}_{TD,L} &= -\frac{3}{4}\rho_G\frac{C_D}{d_G}|\boldsymbol{u}_G-\boldsymbol{u}_L|\left(\frac{\overline{\alpha_G^{'}u_G^{'}}}{\alpha_G}-\frac{\overline{\alpha_L^{'}u_L^{'}}}{\alpha_L}\right)\\ &= -\frac{3}{4}\rho_G\frac{C_D}{d_G}|\boldsymbol{u}_G-\boldsymbol{u}_L|\frac{\nu_{SGS}}{\sigma_{SGS}}\left(\frac{\nabla\alpha_G}{\alpha_G}-\frac{\nabla\alpha_L}{\alpha_L}\right).\end{aligned} \tag{7}$$

Since $\alpha_L+\alpha_G = 1$ in this two-phase flow system and $\nabla\alpha_L + \nabla\alpha_G = 0$, this would yield Eq. (8):

$$\boldsymbol{M}_{TD,L} = -\frac{3}{4}\rho_G\frac{C_D}{d_G}|\boldsymbol{u}_G-\boldsymbol{u}_L|\frac{\nu_{SGS}}{\sigma_{SGS}}\left(\frac{1}{\alpha_L}+\frac{1}{\alpha_G}\right)\nabla\alpha_G. \tag{8}$$

As mentioned in Section 1, the deformation of bubbles can be thought of as a result of the interactions between bubbles and the surrounding turbulent eddies in the frame of Eulerian-Eulerian modelling, which gives rise to the bubble cluster fluctuation. Following the previous work of Long et al. [25] by considering bubble dynamic response to the shear caused by turbulent eddies acting on the bubbles, the liquid-phase turbulence eddy viscosity can be modified as the sum from the filtered turbulent shear and dynamic SGS eddy viscosities, which is written as,

$$\mu_{T,L} = \rho_L(C_s\Delta)^2|S|(1+\mathrm{C_b}\alpha_G\frac{\lambda}{d_B}\left(\frac{1}{1+St_{SGS}}\right)^{\frac{3}{2}}) \tag{9}$$

where λ represents the different turbulent length scales in the range between the integral and Kolmogorov scales ($L>\lambda>\eta$), Cs is a model constant, S is the characteristic filtered rate of strain tensor and St_{SGS} is the non-dimensional Stokes number expressed as $St_{SGS} = \frac{\tau_{\mathrm{bubble}}}{\tau_{L,SGS}}$. Here, the bubble response time scale is proposed by Sommerfeld et al. [41], $\tau_{\mathrm{bubble}} = \frac{4(\rho_G+0.5\rho_L)d_B^2}{3\mu_L C_D Re_B}$. The turbulent eddy turn-over time in sub-grid scale can be estimated by $\tau_{L,SGS} = \Delta/\boldsymbol{u}^{'}_{\mathrm{L,SGS}}$, where $\Delta = \left(\Delta_i\Delta_j\Delta_k\right)^{1/3}$ is the

(a)

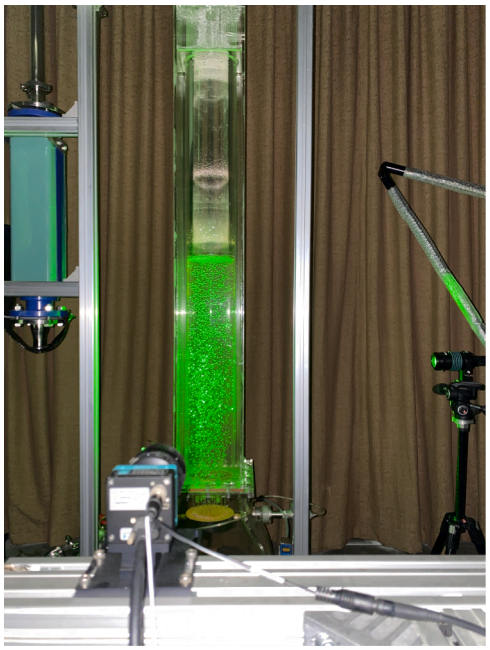

(b)

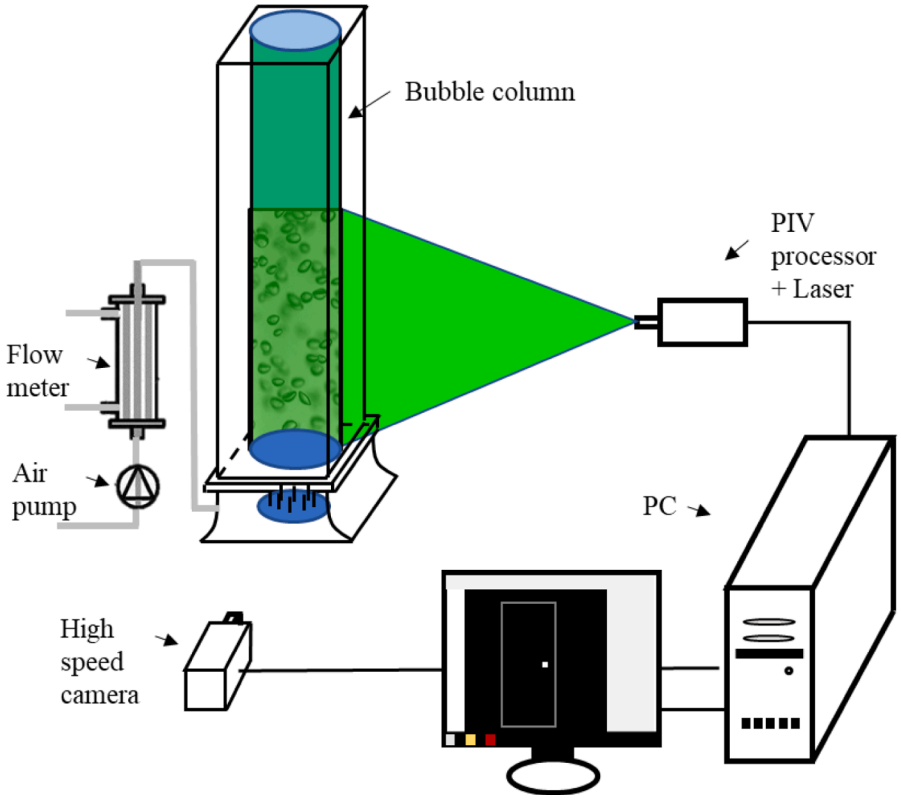

Fig. 3. (a) Experimental set-up of the bubble column and (b) Schematic of bubble column with imaging system and data acquisition.

filter width and $u'_{L,SGS}$ stands for the liquid fluctuation velocity in local grid. That $\lambda \sim \Delta$ is assumed since the filter length scale is usually falling into the range of inertia subrange wave length of turbulent kinetic energy spectrum. Thus, the turbulent dispersion considering turbulent eddies interaction with bubbles, which may give rise to bubble deformation or oscillation in bubble column bubbly flow can be evaluated by

$$\boldsymbol{M}_{TD,L} = C_{TD}\frac{3}{4}\rho_G\alpha_G\frac{C_D}{d_G}|\boldsymbol{u}_G-\boldsymbol{u}_L|\frac{(C_s\Delta)^2|S|\left(1+C_b\alpha_G\frac{\Delta}{d_B}\left(\frac{1}{1+St_{SGS}}\right)^{\frac{3}{2}}\right)}{\sigma_A}\left(\frac{1}{\alpha_L}+\frac{1}{\alpha_G}\right)\nabla\alpha_L. \quad (10)$$

It can be seen that the effect of sub-grid scale bubble induced turbulence on SGS turbulent dispersion and viscosity has been incorporated into Eq. (10). Eq. (10) will be implemented into the present LES simulations and it is referred to as the modified sub-grid turbulent dispersion force model (SGS-TDF).

2.2. Numerical modelling and experimental study

The reliability of the proposed SGS turbulent dispersion model was validated by comparing the simulation results with the detailed experimental data as reported by Sommerfeld et al. [41] and the author's repeated experiment using the PIV. The experiments were repeated in the author's laboratory based on the same experimental condition and bubble column configuration as that carried out by our German research collaborator (Sommerfeld *et al.*, 2009). Both the modelled circular bubble column and the actual bubble column used in the experiments have an internal diameter of 140 mm, which was filled with liquid at a static height of 0.65 m (Fig. 3(a)). The experimental bubble column has a gas sparger that contains 50 evenly distributed capillaries at 0.4 mm in diameter, injecting the gas from the annular region within 100 mm in diameter. The detailed operation parameters for the selected case are listed in Table 2.

Table 2
Operation parameters adopted for the bubble column bubbly flow.

Gas flow rate (l/h)	160
Global gas hold-up (%)	1.26
BSD weighted bubble diameter (mm)	2.55
Bubble column diameter (m)	0.14
Static liquid height (m)	0.65
Observation height (m)	0.325

Air was injected with superficial velocity of 160L/h into the system to provide a steady flow profile, the gas hold-up was controlled at 1.26 %. In order to obtain the bubble velocity and bubble volume fraction distribution, both PIV (Dantec Dynamics) and high-speed camera (Nikon AF-S 24 mm f/1.8G ED) were applied as shown in Fig. 3(b). The PIV equipment is composed of a Nd:YAG laser, a CCD camera, a timer box and the Dynamic-Studio software. The laser sheet illuminates the tracer particles on a sheet of light plane. The camera is positioned in the vertical direction of the sheet light plane. The computer uses related algorithms to compute the velocity vectors from each image pair. For all experiments, the images are acquired by high-speed camera at a rate of 2000 frames (1000 image pairs) per second and a total scanning period of 10 s. Fig. 4 shows the images of bubbles captured at the central region of the bubble column in the original format and the resolved version after filtering the image by coding in MATLAB, ensuring the individual bubbles in the illustrated plane by the laser are discernible. The vertical compression of bubbles in the experiment is primarily caused by the joint influences contributed from the hydrostatic pressure changes and the resistance together with the added mass stress force variation during the process of bubble's ascending. The velocity profile was obtained by evaluating the double frames using the PIV, as shown in Fig. A1. The velocity vectors obtained from the instantaneous images can be used to calculate the mean and fluctuation, which can give out the turbulence characteristics of the bubble flow in the bubble column.

The same measured number weighted bubble size distribution (BSD) among the entire bulk phase obtained in the experiment was adopted in the LES modelling but subjected to adjustment as discussed later in this section. A good prediction of the BSD is crucial for estimating the interfacial area, which directly has an impact on calculating the thermal and mass transfer rate in the bubble column reactor. In the previous studies on bubble column bubbly flow, a Gaussian distribution of the BSD at the bubble column inlet area was assumed for various configuration of bubble distributors or spargers and applied for different superficial velocity conditions [33]. As an example, Polli et al. [33]

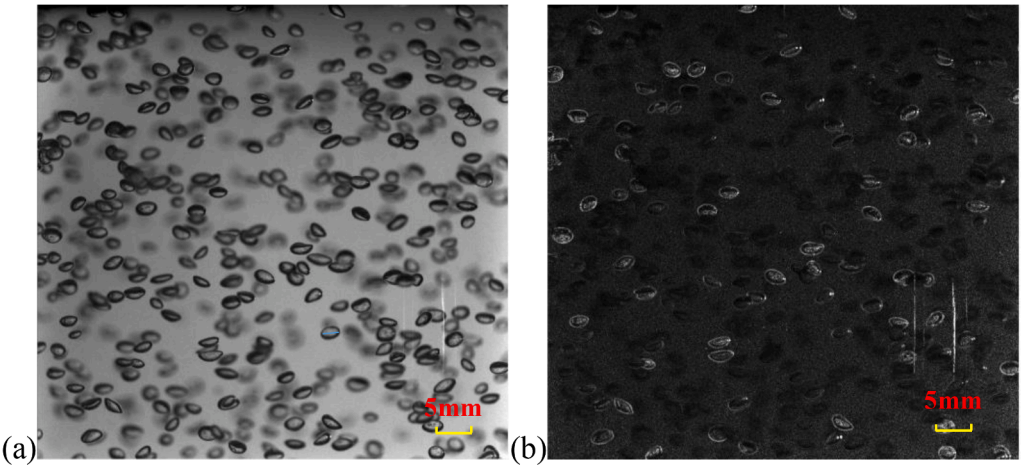

Fig. 4. Typical image of bubbles in the central region (a) original image; (b) resolved image by sharpness (individual bubbles in the illustrated plane by the laser are discernible). The focal length used in the experiment was 94 mm.

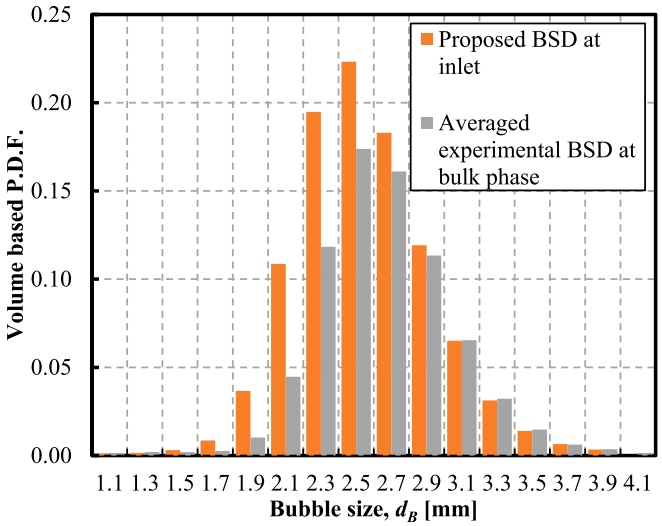

Fig. 5. Comparison of domain-averaged BSD and the adjusted BSD employed in the present LES simulation. (Grey: experimental domain-averaged BSD at bulk phase (Sommerfeld et al., 2009); Orange: adjusted BSD at inlet in this work). (For interpretation of the references to colour in this figure legend, the reader is referred to the web version of this article.)

suggested an empirical correlation for approximately estimating the bubble size distribution at the gas distributor,

$$f_i = q \bullet \exp\left(-\frac{(d_i - \overline{d})^2}{\left(\gamma^p d_{i,min}^3\right)^{2/3}} \right) \tag{11}$$

where, i denotes the i-th class of bubbles at the sparger region, f represents the void fraction of the i-th class of bubbles and d stands for the bubble diameter. $\overline{d}$ denotes the bubble mean diameter, p and q are the coefficients which satisfy the requirement of $\sum_{i=1}^{n} f_i = 1$. γ stands for the volume increment ratio. In general, the original BSD must be related to the quantity and the diameter of the sparger capillaries, properties of the carrier phase and superficial velocities. It was found from the trial simulations that the use of the correlation between f_i and $\overline{d}$ together with γ as given by Eq. (11) may be much more efficient in LES modelling.

After considering the condition of the gas sparger used in the experimental set-up and the correlations suggested for the inlet superficial velocity and those BSD adopted in the previous studies [20,2,47], the adjusted BSD at the inlet is proposed and employed in the homogeneous Multiple Size Group Model (MUSIG) in this LES work. Due to the inevitable influence of pressure drop, bubbles experience a slight volume increase during their ascent. Therefore, it is unreasonable to directly use the domain-averaged distribution as the inlet bubble size distribution (orange) in the simulation. MUSIG model allows for the simulation of poly-dispersed bubbly flows and incorporates the population balance approach, which enables the description of binary bubble coalescence and breakup (Liao, 2020). Bubbles from 1.1 mm to 4.1 mm diameter are divided into 16 groups sharing the same inlet velocity, the corresponding size function can be found in Fig. 5. It should be noted here that during the bubble rising up to the liquid top surface in the bubble column, they may coalescence with other bubbles or break up. Consequently, these interactions within the reactor can produce bubbles of different diameters, shapes and velocities. Yet, when talking about the homogeneous regime in bubble column reactor i.e., $\alpha_G < 0.04$, the diameters of the bubbles and the slip velocities are nearly the same for bubbles transported in the column. Apart from these, bubbles move with small collision, breakup and coalescence rates [35]. If no coalescence and breakup occurrence is assumed, the bubble number density equation can be expressed by

$$\frac{\partial n}{\partial t} + \nabla \bullet (\boldsymbol{u}_G \mathrm{n}) = 0. \tag{12}$$

The Sauter mean diameter can then be obtained by

$$d_{G32} = \left(\frac{6\alpha_G}{\pi n}\right)^{1/3}. \tag{13}$$

It can be assumed that the local bubble equivalent diameter's variation is the same order of the level of grid scales, therefore, the bubble size can be characterised with the 0-th moment of the bubble size distribution i.e., only taking the local mean bubble diameter. Thus, one mean bubble diameter rather than a range of bubble sizes can be specified. This approach requires much less computational effort and offers a surprisingly good agreement with available experimental data in comparison with other ways for evaluating bubble sizes such as the adoption of population balance model (PBM) [17].

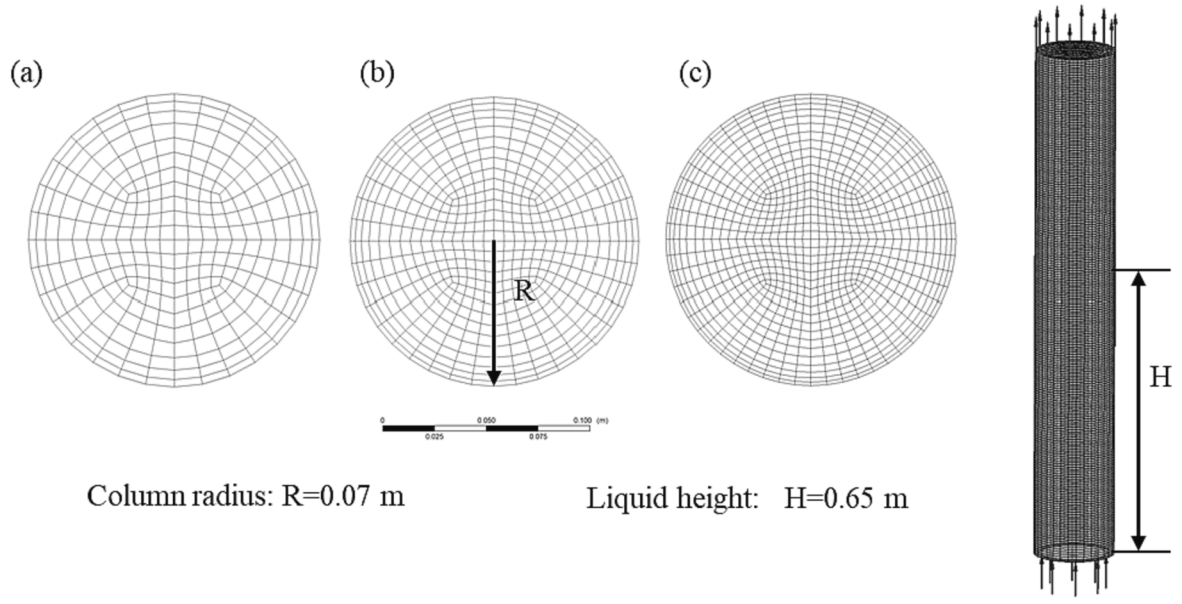

Fig. 6. Schematic of the mesh set-up (a) $\frac{d_{mean}}{\Delta} = 0.51$ (b)$\frac{d_{mean}}{\Delta} = 0.6375$ (c) $\frac{d_{mean}}{\Delta} = 0.85$ and the bubble column configuration used in the simulations of the resent study.

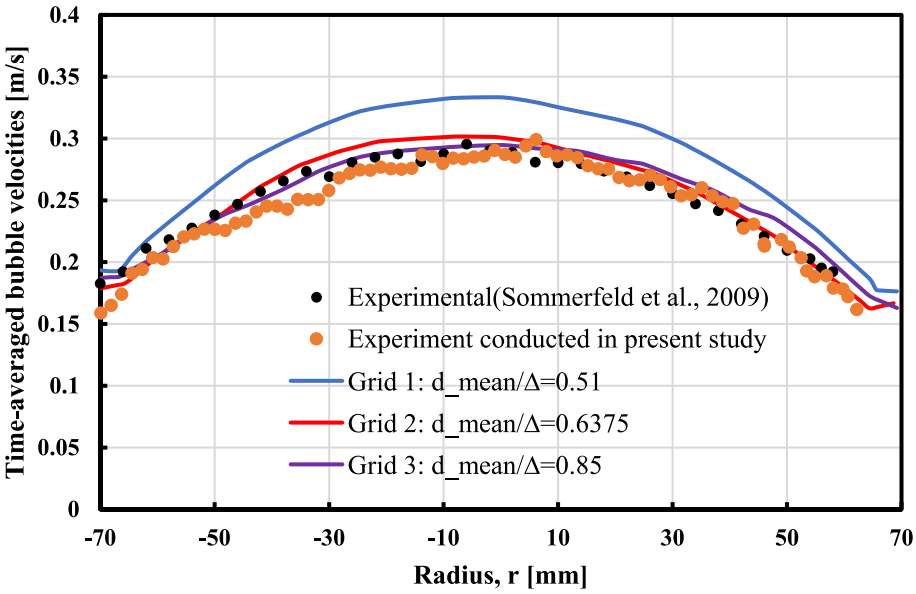

Fig. 7. Grid independence analysis by employing modified SGS-TDF with adjusted BSD at inlet at z = 325 mm. (Blue: Fig. 4(a); Red: Fig. 4(b); Purple: Fig. 4(c)). (For interpretation of the references to colour in this figure legend, the reader is referred to the web version of this article.)

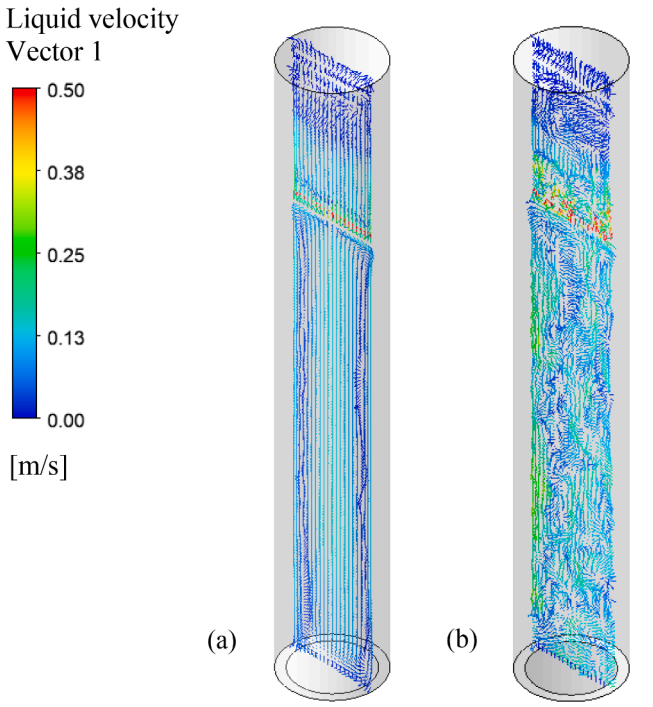

Fig. 8. Liquid axial velocity field in the bubble column. (a) Time-averaged velocity field; (b) Instantaneous velocity field at 100 s.

ANSYS CFX 2021R1 with compiled CCL is employed for Euler/Euler LES modelling in the present study. The boundary conditions are set as follows. At inlet, a mass flow rate perpendicular to the inlet is adopted, which is corresponding to the experimental conditions as reported in Sommerfeld *et al.* (2009), and the volume fraction for each phase is specified as : $\alpha_L = 0, \alpha_G = 1$. At the top surface of the reactor, a pressure-constant boundary, i.e., relative pressure being specified to be 0, is used. A non-slip condition is used for the inner wall of the bubble column. A central-differencing discretisation scheme is used for the momentum equations, while a second-order backward Euler scheme is employed regarding to the discretization algorithm for the transient term in all of the simulations. The mesh set-up for the current LES modelling is illustrated in Fig. 6. The bubble column was discretised with the cell size of $\Delta x^+ = 100$ and $\Delta r^+ = 5$ with growth rate of 1.2. In order to validate the proposed SGS-TDF model, the mesh independency was check with $\frac{d_{mean}}{\Delta} = 0.51$, 0.6375 and 0.85 in the cross section at z = 325 mm of the bubble column as shown in Fig. 6. The time-averaged bubble velocities at middle point at z = 325 mm obtained from three mesh set-up cases are compared with the experimental results obtained from the present study and carried out by Sommerfeld *et al.* (2009). The time averaged velocity is calculated by using the relationship given by

$$\overline{u_B} = \frac{1}{N\Delta t}\sum_{i=1}^{N} \boldsymbol{u_{Bi}}(r,t)\Delta t$$

where $\overline{u_B}$ represents the time-averaged bubble velocity, N stands for the number of the collected samples, Δt is the sampling time period. Close inspection of the Fig. 7 shows that the predicted results employing three grids follow the trend of the experimental axial bubble velocity. No notable variations are found between the mesh of $\frac{d_{mean}}{\Delta} = 0.6375$ and the finer one. Both grids produce results that are in good accord with the experiments when comparing to the coarser grid $\frac{d_{mean}}{\Delta} = 0.51$. Details on simulation results utilising the modified model will be discussed in the following section. Regarding to the more accurate predictions of the axial bubble velocity, which are compatible with the experimental values. With caution and the perspective of the computational cost, $\frac{d_{mean}}{\Delta} = 0.6375$ in the core-region was used in the current Eulerian-Eulerian LES modelling. The grid resolution adopted in the simulation is considered reasonably close to Milelli's limit (Milelli, 2002). By using this mesh set-up, the control volume cell size is and large enough to contain the interface details and fine enough to resolve large scale turbulence. The mesh set-up with 95,400 cells was thus adopted throughout our LES simulations.

3. Results and discussion

Two scenarios have been studied using the Euler/Euler LES by adopting the uniform bubble diameter $d_b = 2.55$ mm and the MUSIG model but with the BSD specified according to the experiment for the bubble column sparger inlet, respectively. In the simulations, the cases with and without considering the turbulent dispersion force model have

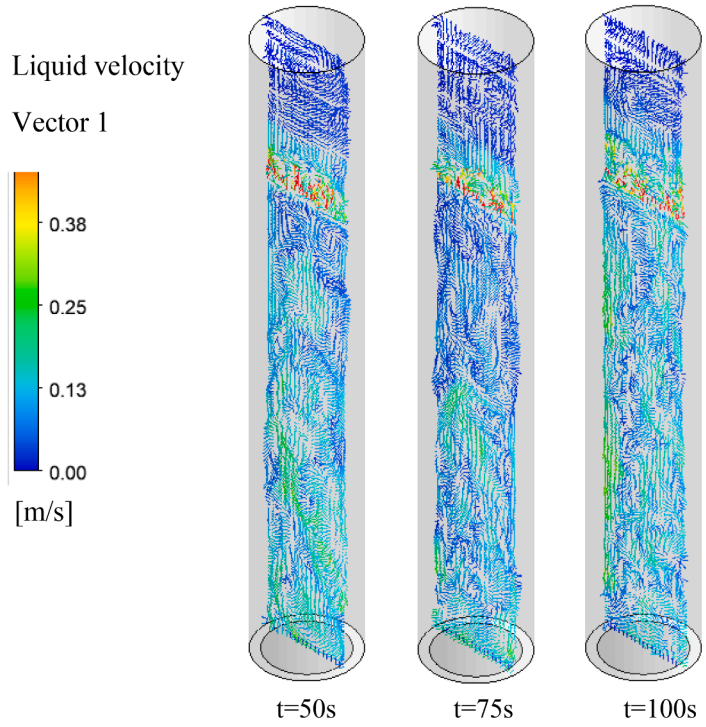

Fig. 9. Instantaneous liquid phase velocity distribution at different times, obtained in the cutting plane of the bubble column.

been particularly investigated. The time step is set in terms of the CFL criterion, min $(\frac{|u_L|\delta t_E}{\Delta}, \frac{|u_G - u_L|\delta t_E}{\Delta}) < 0.03$, varying from 0.0005 s to 0.001 s for capturing the transient behaviour of turbulent shear eddy evolution in the bubble column. The simulations were run to last for 100 s while the instantaneous velocities at given positions were monitored and recorded during the calculation process. In order to obtain the turbulence statistical characteristics, the time average was taken over a period of 50 s after the bubbly flow fluctuation patterns have been well established, i.e., about 4 periods have been achieved.

3.1. *Effects of accounting for the turbulent dispersion in LES on bubble transport*

Fig. 8 shows the normalised time-averaged liquid axial velocity and instantaneous velocity field in the cutting plane of the bubble column. Since the unsteady turbulence prediction from LES can better resolve most large-scale turbulence in space and time, the time-averaged results of LES for liquid velocity and residence time can be used to estimate the large turbulent eddy length and time scales, which is approximately the Taylor integral scale for the bubble column reactor. For bubble column bubbly flow, it has been observed that the existence of a wide range of length and time scales affects the transport processes in the bubble column. This can be regarded as the combination of four flow patterns, including the descending flow, large eddy spiralling, fast bubble rising and central pluming. As can be seen from Figs. 8 and 9, the LES simulation using the modified SGS-TDF model captured well the characteristics of the ascending gas–liquid two-phase flow in the bubble column. The instantaneous velocity vector field at t = 50.0, 75.0, and 100.0 s, highlighted by the instantaneous bubble volume fraction, clearly shows the bubble spirally rising induced flow. It can be seen from the figure that the descending flow takes place near the wall, characterised by the downward velocity vectors while higher bubble void fraction occurring at the centre of the column points out that the bubbles are collected and entrained by the central large turbulent eddies. At t = 50.0, 75.0, and 100.0 s, it can be seen clearly that there are a number of large eddies fluctuating in the entire liquid zone, accompanied by time-dependent fluctuations of the bubble volume fraction contours. Figs. 9 and 10 serve to demonstrate the capability of our LES approach to capture transient turbulent flow behaviour. It can be seen from the figures that the visualizations reveal the dynamic nature of the eddies within the flow, showcasing their continuous fluctuations in response to changes in both time and positions. The figures also unveils the intricate interplay between these eddies and the evolving flow field, providing valuable insights into the temporal and spatial characteristics of the turbulent phenomena under investigation.

To highlight the importance of the turbulent dispersion effects on the bubble transport in Eulerian-Eulerian LES modelling, the results obtained by using our modified SGS-TDF model are also compared with Euler/Lagrange LES simulation results [41] as shown in Figs. 10 and 11. In Fig. 10, the time-averaged bubble and liquid axial velocity profiles predicted by using the modified and standard turbulent dispersion force models at height $z = 0.325$ m are illustrated. The experimental results and the Eulerian-Lagrangian simulation results carried out by Sommerfeld et al. [41] are also presented for comparison. According to their Euler/Lagrange simulation, the interfacial forces such as drag, wall lubrication, lift, buoyancy, and added mass forces were accounted. The Euler/Euler LES simulation in this work employed the forces that include the time averaged drag, lift, buoyancy, added mass forces together with the use of the modified SGS-TDF bubble turbulent dispersion, taking into account bubble induced turbulence (Cases 2 and 4). Since the standard turbulent dispersion force is modified with the consideration of bubble response to eddies, the result obtained for Case 4 can be therefore compared with Case A of Sommerfeld et al. [41]. Moreover, an additional factor with bubble shape change, i.e., the ratio of the long to short axis of the bubble, for bubble oscillation was considered in their simulation (Case B). It can be seen from Fig. 10 that the use of adjusted BSD at inlet for our Euler/Euler LES by implementing either the modified or standard SGS-TDF force model (Cases 3 and 4) performs better than the simple use of one bubble diameter (Cases 1 and 2) for the prediction of both liquid and bubble velocity profiles. It is worth noting that the transient behaviour of different sizes of bubbles is actually different from the one described by specifying an equivalent mean bubble size. Here, the findings imply the significance of adopting a multigroup sizes of bubble diameter model.

When restricting the attention to the results using the MUSIG approach (Cases 3 and 4), the predicted bubble axial velocity profile is in good agreement with the experimental data as reported by Sommerfeld et al. [41]. It can be seen from Fig. 10 that the liquid axial flow is distinctly upward in the central region, while a descending flow can be observed in the vicinity of the wall, consistent with the trend based on the experimental observation. The position of flow reversal is clearly seen to take place at a radial location of around $r/R = 0.6$–0.8. The bubble velocity profile predicted by neglecting the SGS-TDF contribution (Case 3) shows a greater difference from the experimental result. This clearly demonstrates that the inclusion of the modified SGS-TDF in LES simulation has a remarkable influence on the bubble radial migration. It should be noted that the consistency of Euler/Euler LES modelling results on predicted liquid phase axial velocity and volume fraction profiles compared with the experimental data are slightly poor in the central region of the bubble column but becomes good in the near-wall region. This may be attributed to the fact that bubbles are more likely to coalescence in the central region where the equivalent bubble diameter d_B may change quite a lot. While an approximate bubble size of 4 mm was allocated in this region, which corresponds to $\frac{d_B}{\Delta} \in (0.875, 1.025)$ and has violated the criterion of Milelli *et al.* (2002), the use of BSD may overestimate the bubble fluctuation in the main flow direction so that the induced liquid velocity may be slightly overestimated. On the other hand, relatively small bubbles are likely to accumulate near the wall region, which are very sensitive to the surrounding turbulent eddies. This further indicates that the use of the modified SGS-TDF model has a function that modulates the bubble dispersion behaviour, consequently giving rise to a better estimation of the void fraction gradient and a better prediction of the bubble lateral dispersion. Based on the comparison with Euler/Lagrange LES results (Case B) of Sommerfeld et al. [41], it has been shown that our Euler/Euler LES coupled with the modified SGS-TDF model can still give consistent results for bubble dynamics when comparing with the experimental data. In terms of the averaged radial velocity as shown in Fig. 10(b), the radial distribution in all three cases relatively agrees with the experimental data. On average, case 4 exhibits lower values. The negative radial velocity observed in

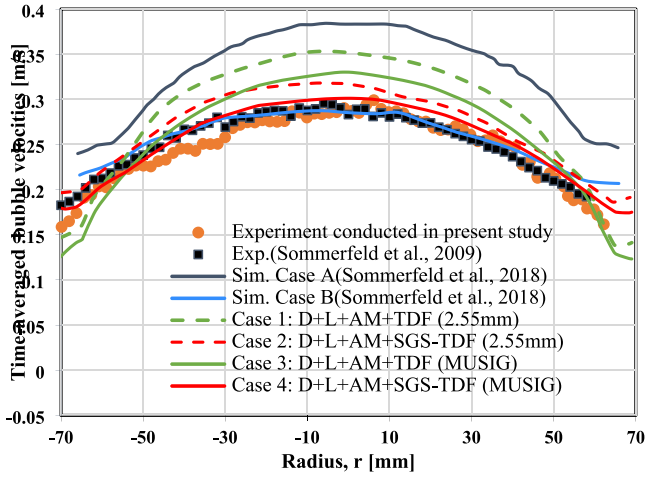

(a)

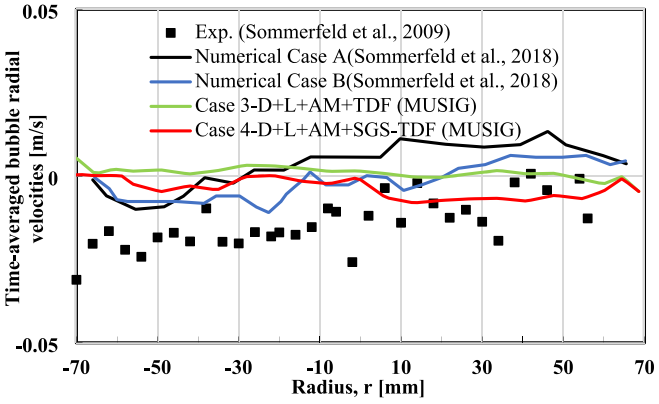

(b)

Fig. 10. Comparison of LES predicted time-averaged liquid and bubble velocity profiles at the cross-section z = 325 mm. (a) Bubble axial velocity distribution; (b) Bubble radial velocity distribution; (c) Liquid axial velocity distribution.

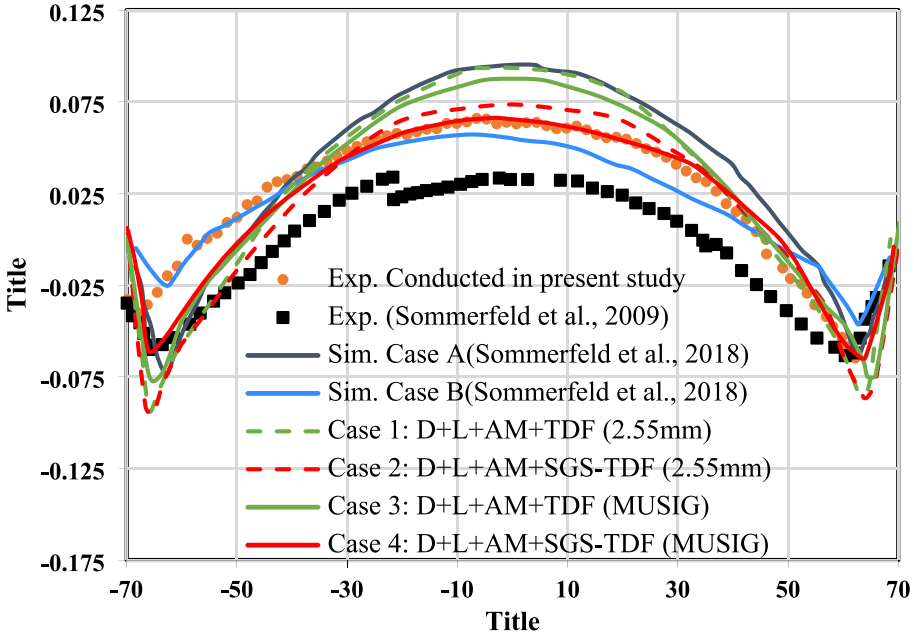

(c)

Fig. 10. (*continued*).

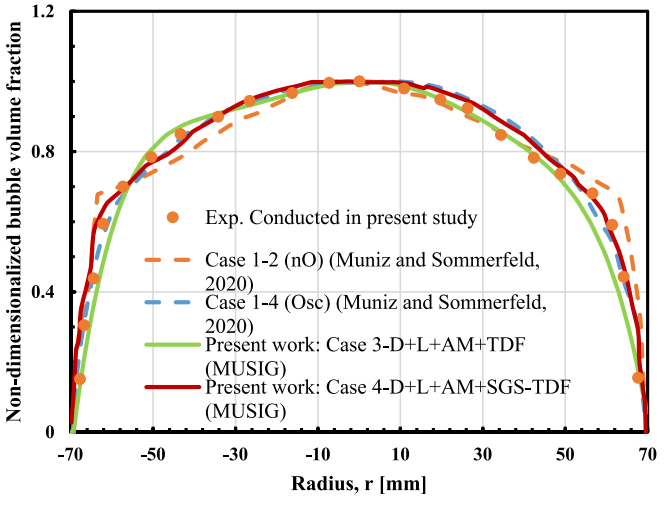

Fig. 11. Comparison of Euler/Euler LES (present study) with Euler/Lagrange LES [31]for the predicted time-averaged bubble volume fraction profiles at z = 325 mm. Labels: nO: no bubble dynamics model; Osc: with bubble dynamics model.

Fig. 10(b) is indeed an interesting observation and can be explained in the context of the momentum transport equation. The equation, $\frac{\partial}{\partial t}(\alpha_k\rho_k\boldsymbol{u}_k) + \nabla\bullet(\alpha_k\rho_k\boldsymbol{u}_k\boldsymbol{u}_k) = -\nabla\bullet(\alpha_k\tau_k) - \alpha_k\nabla p + \alpha_k\rho_k g + \boldsymbol{M}_{F,k}$, describes the transport of momentum in the fluid phase. In short sampling times, the first term on the left side of the equation can be disregarded. Breaking down the equation, we find that $\frac{\partial u_k u_k}{\partial r}$ represents the change in radial velocity with respect to radius. The negative radial velocity can be attributed to the following factors: 1) The negative sign associated with the shear stress term indicates that it acts to decrease radial velocity. This is typical in regions where there is a significant velocity gradient, such as near the wall. 2) Pressure Gradient ($-\alpha_k\frac{\partial p}{\partial r}$): In the central region of the bubble column, where flow velocity is high and pressure is low, the pressure gradient should be directed towards the center. Considering the negative sign, this also contributes to the negative radial velocity. 3) downward gravity leads to a negative sign. 4) interfacial force terms: Drag tend to oppose the bubble's upward motion, contributing to the negative value. And lift force tend to point to the wall, which contributes to a negative value. Added mass force accounts for the impact of the bubble's motion on the local fluid vortices, which can also act to reduce radial velocity. The SGS-TDF term represents the effect of subgrid-scale turbulence and dispersion, which can lead to a reduction in radial velocity. In summary, the negative radial velocity observed in Fig. 10(b) can be explained by the complex interplay of various forces and gradients in the bubble column. It is worth noting that experimental errors may also be present due to insufficient sampling time or operational inaccuracies.

Fig. 11 shows the time-averaged radial bubble volume fraction distribution obtained by using the standard SGS-TDF and modified SGS-TDF models. These are marked as cases 3 and 4, compared with the Euler/Lagrange LES simulation results reported by Muniz and Sommerfeld [31]. It is worth mentioning that the adoption of the bubble dynamic model has significantly improved the simulation results and were in reasonable agreement with the experimental data in their work. The two dash lines represent the predicted bubble volume fraction with (blue) and without (orange) bubble dynamics model. The prediction of bubble void fraction profiles can be used as an indicator to assess the predictability of the proposed TDF model. It can be observed that the predicted profile by using the modified SGS-TDF model is comparable to the blue dashed line, and consistent with the bubble velocity profiles (Fig. 10). Compared to the non-modified SGS-TDF model, a noticeable improvement was found especially in the near-wall region although the magnitude of contribution from the turbulent dispersion force predicted using the modified SGS-TDF was small compared to the other forces. The fact that the results obtained by considering the fluctuating $\overline{\alpha_k'\boldsymbol{u}_k'}$ with dynamic response to surrounding eddies were improved and most consistent with the experimental results highlights the need for the inclusion of SGS-TDF for accurate modelling of bubble dispersion especially bubble radial migration in the bubble column bubbly flow. It can

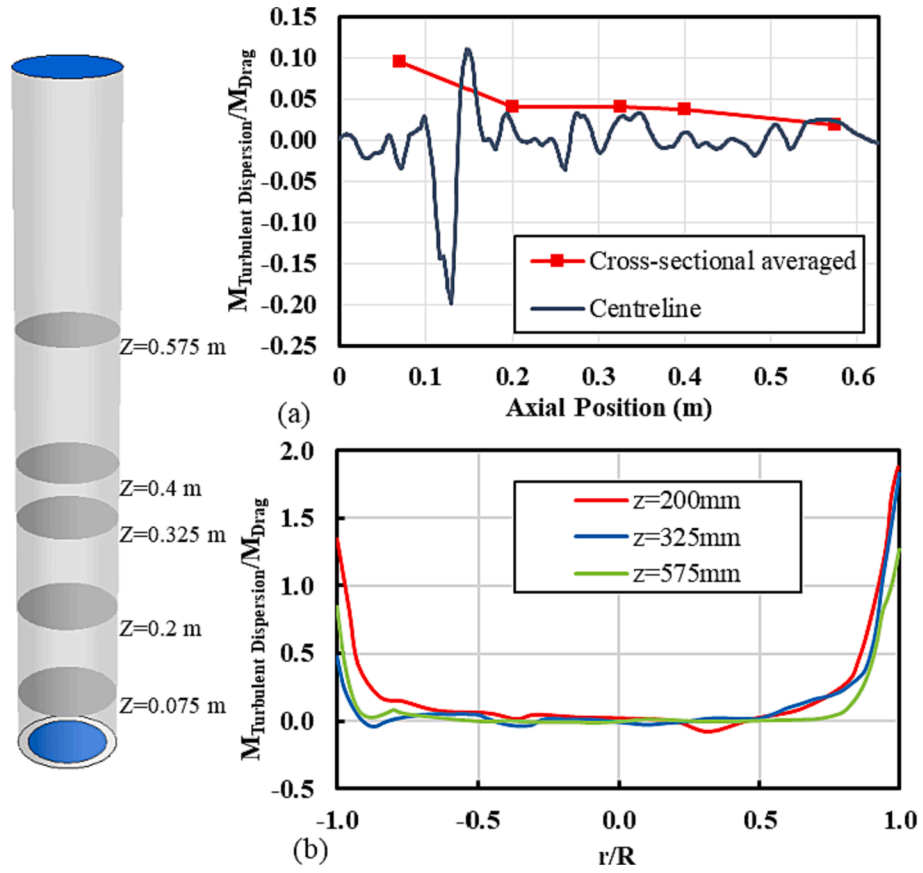

Fig. 12. Quantification of SGS turbulent dispersion force (TDF) contribution: (a) instantaneous SGS-TDF/Drag force along centreline and cross-sectional averaged ratio at different cross-sections along the bubble column height at 100 s. (b) Time-averaged SGS-TDF/Drag force ratio in radial direction at different cross-sections along the bubble column height.

be cautiously inferred that the bubble lateral dispersion effect may be highly associated with the bubble oscillations as the filtered turbulent eddy fluctuations bring out the bubble surface deformation if there is no coalescence occurring (see Figs. 1 and 2).

3.2. Quantification of SGS-turbulent dispersion force contribution and its effect on bubble oscillation

In the preceding section, $\overline{A_k' u_k'}$ has been identified to be related to filtered eddy fluctuation induced turbulent dispersion and it has a potential impact on turbulent eddies interaction with bubbles, which may result in the change of bubble interfacial area. With the eddy diffusivity hypothesis, the relationship between the SGS area density fluctuation and relative velocities can be considered analogous to the relationship between volume fraction and fluctuation velocity as expressed by Eq. (14)

$$\frac{\overline{A_{GL}'(\boldsymbol{u}_G' - \boldsymbol{u}_L')}}{\overline{A_{GL}}} = \frac{\overline{\alpha_G'(\boldsymbol{u}_G' - \boldsymbol{u}_L')}}{\overline{\alpha_G}}. \tag{14}$$

For the derivation of Eq. (14), it was assumed that the bubble diameter is unchanged by using Eq. (3). If no constraint is applied, Eq. (14) can be approximated:

$$\frac{\overline{\alpha_G'(\boldsymbol{u}_G' - \boldsymbol{u}_L')}}{\overline{\alpha_G}} \approx \frac{\overline{(A_{GL} d_B)'(\boldsymbol{u}_G' - \boldsymbol{u}_L')}}{\overline{(A_{GL} d_B)}}. \tag{15}$$

In fact, the bubbles would change their shapes in the duration of the rise-up in the bubble column, which would be characterised by the interfacial area and equivalent diameter variations. Thus, Eq. (15) implicitly indicates the behaviour of instantaneous bubble shape variations in the bubble column. In order to characterise the contribution from turbulent dispersion, the ratios of turbulent dispersion force and dominant drag force at different cross-sections along the height of the bubble column are shown in Fig. 12. The radial turbulent dispersion force component at a given height has been obtained by the following averaging method.

$$\boldsymbol{M}_{TD,L}(\mathrm{r,\ z}) = \frac{1}{2\pi r}\int_0^{2\pi} \left[C_{TD}\frac{3}{4}\rho_G \alpha_G \frac{C_D}{d_G}|\boldsymbol{u}_G - \boldsymbol{u}_L| \frac{(C_s\Delta)^2|S|\left(1 + C_b\alpha_G^{\frac{1}{3}}\left(\frac{1}{1+St_{SGS}}\right)^{\frac{3}{2}}\right)}{\sigma_A}\left(\frac{1}{\alpha_L} + \frac{1}{\alpha_G}\right)\nabla\alpha_L \right] r d\theta \tag{16}$$

In this equation, various parameters and terms contribute to the calculation of the radial turbulent dispersion force component. The integration is performed over the azimuthal angle θ to sum and average the force exerted in the radial direction $\boldsymbol{M}_{\mathrm{TD,L}}$ (Eq. (10)) at each angle at a given height (z). The turbulent dispersion resulting from sub-grid eddies cannot be experimentally measured or validated at the current stage. Fig. 12 shows the quantification of the sub-grid turbulent dispersion force (instantaneous and filtering-averaged). By comparing the magnitude and the directional dominance in relation to drag force, the relative influence of filtering-averaged SGS-TDF within the particular flow system can be scaled. Fig. 12(a) shows the ratio of instantaneous SGS-turbulent dispersion force to drag force along centreline and the cross-

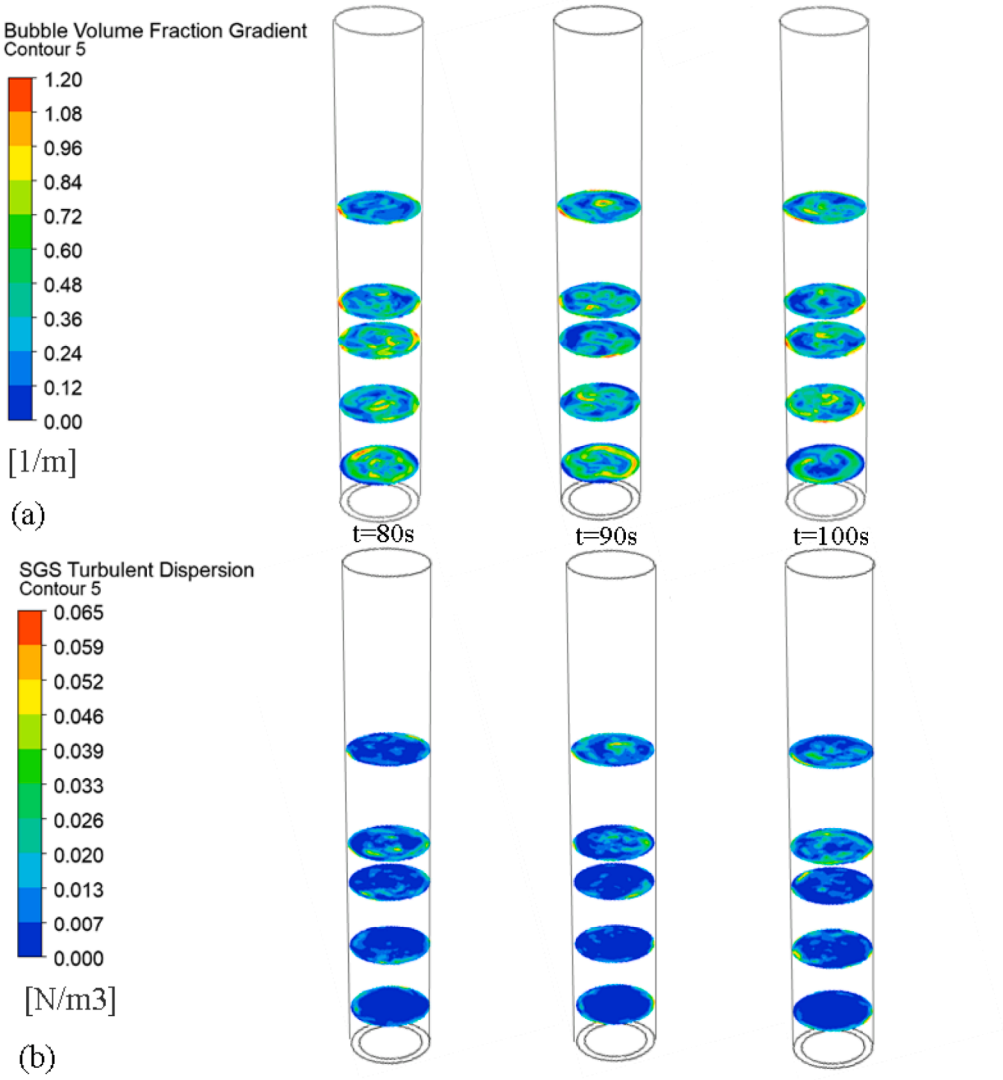

Fig. 13. Instantaneous contour plots of bubble volume fraction gradient and instantaneous SGS turbulent dispersion force per unit volume at different cross-sections along the bubble column height at different time. (a) t = 80 s; (b) t = 90 s; (c) t = 100 s.

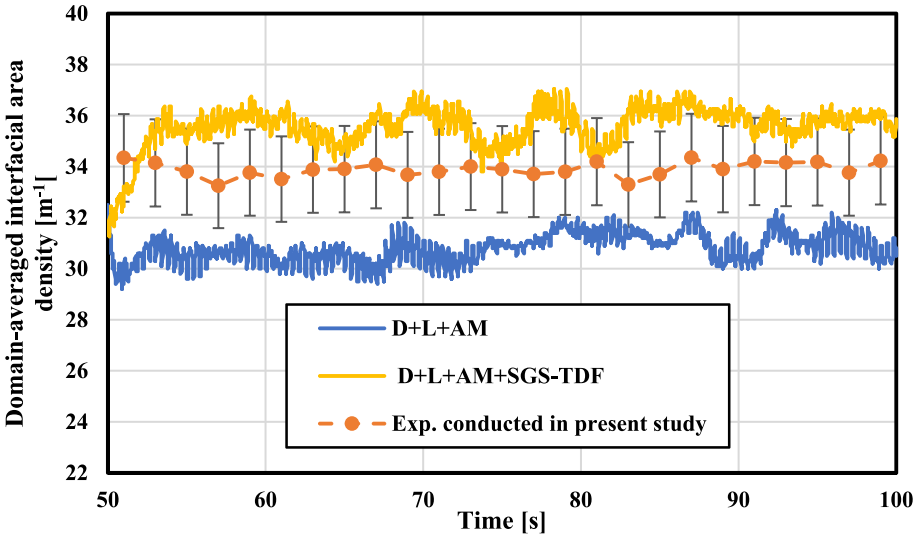

Fig. 14. Time history of the predicted domain-averaged interfacial area density.

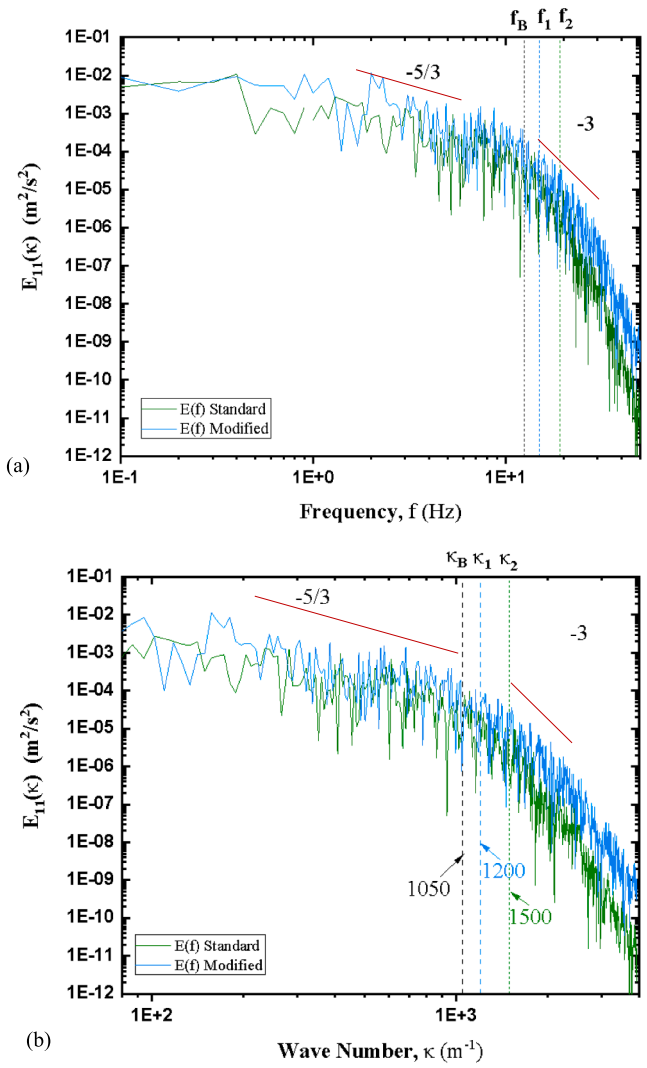

Fig. 15. Turbulent kinetic energy spectrum of liquid axial fluctuation velocity: (a) change with frequency; (b) change with wavenumber, extracted from the location in the centreline at z = 325 mm.

sectional averaged ratio at different cross-sections along the bubble column height at 100 s. It can be seen from the figure that along the centreline, the absolute ratio of SGS-TDF to drag can reach 20 %. Furthermore, a cross-sectional averaged ratio of 10 % is reached at z = 0.075 m and the force ratio around 5 % is remained along the height of the column. The decrease in the ratio of instantaneous SGS-turbulent dispersion force to drag force along the column height reveals that the bubble lateral dispersion is highly associated with the bubble cluster oscillations. It should be noted that turbulence generated in the vicinity of the gas distributor has a higher intensity, which causes a higher frequency of bubble oscillations. Fig. 12(b) shows the radial distribution of the ratio of time-averaged SGS-TDF to drag at z = 0.2, 0.325 and 0.575 m, respectively. It becomes clear that the ratio is usually greater in the vicinity of the wall at each axial position, which further demonstrates the effect of the modified SGS-TDF term on bubble lateral dispersion. In terms of the ratio profile at z = 0.2 m, the SGS-TDF magnitude can be even 1.7 times greater than the averaged drag force in the lower part of the bubble column. Apparently, high correlation of the bubble oscillation with the bubble dispersion does exist while the effects of SGS-turbulent dispersion force may retard the bubble cluster oscillation close to the wall, as evidenced by a larger ratio of SGS-TDF/Drag occurring with increase of the radial position. According to most of previously reported studies, the drag force can take around 60 %–80 % of all the considered interfacial forces [31]. Thus, the present study has highlighted the importance of the contribution of SGS-TDF. This finding is also supported by the contours of the bubble volume fraction gradient and SGS-TDF per unit volume, shown in Fig. 13. A closer observation of the contours of the SGS-TDF force and bubble volume fractions indicates that the SGS-TDF is correlated with the variation of the instantaneous dispersed phase void fraction gradient and has a significant impact on bubble transport in radial direction than in the axial direction, i.e. the main flow direction for the bubble column.

Fig. 14 shows the time history of the predicted domain-averaged interfacial area density for two cases with and without considering SGS-TDF (the former includes the drag, lift and added mass forces (D + L + AM) and the latter further adds the SGS-TDF (D + L + AM + SGS-TDF)). It can be seen clearly that by considering the impact of SGS-TDF on the bubble transportations, the predicted domain-averaged interfacial area density is increased by around 19 %. To quantify the contribution due to the bubble deformation caused by turbulent dispersion, one can compare the total interfacial area density obtained from the experimental condition with the ones extracted from the simulations. The experimental data is calculated based on the monitored average liquid level of the dynamic liquid surface after injecting the gas for 50 s, $a_{exp} = \frac{h_{liquid} \times \pi r_{BCR}^2 \bullet \alpha_{G,\ domain\ avg}}{\frac{\pi}{6} d_{32}^3} \times \pi d_{32}^2$. Based on the bubble volume fraction obtained from the simulations shown in Fig. 14, the time-averaged interfacial area for case of considering D + L + AM is estimated to be 30.8 m^2 per unit volume, and 36.0 m^2 for the case D + L + AM + SGS-TDF, corresponding the predicted domain-averaged interfacial area density 0.308 m^2 and 0.360 m^2, respectively, which is consistent with the experimentally estimated total interfacial area density data with an error of 5 % for the latter case. It should be noted here that the experimental domain-averaged interfacial area density, $a_{exp,avg} \approx 0.343$ m^2, was obtained by assuming a single bubble diameter of 2.55 mm without accounting for the actual bubble deformation. Further research is needed in the future to explore more precise methods for measuring interfacial area density. On the other hand, for the second case, considering the term of SGS-TDF in the simulation does show a significant increase in the interfacial area. This indicates that it is crucial to include SGS-TDF in the simulation for better estimating of bubble deformation and better capturing the interfacial mass transfer.

3.3. *Effects of turbulent dispersion on turbulent shear structures and turbulent kinetic energy spectra*

In order to assess the impact of turbulent dispersion on the turbulent kinetic energy of the liquid phase, the one-dimensional LES-filtered turbulent kinetic energy power spectral density (PSD) E(κ) are presented in Fig. 14 with the data extracted for Case 3 and 4. The axial turbulent velocity are monitored at the centre of the cross section at z = 0.325 m. The turbulent energy spectrum is obtained by taking the Fast Fourier Transform (FFT) of the time correlation of axial turbulent velocity fluctuations based on the Welch method (Welch, 1967). The one-dimensional model energy spectrum for single-phase flow as proposed by Pope is also shown in Fig. 15 (Pope, 2001). As can be seen from Fig. 15, the PSD predicted by the modified SGS-TDF model can still be approximated and described by Pope's model spectrum, which is valid in the wide energy spectrum of turbulence. It is defined as,

$$E(\kappa) = C\varepsilon^{2/3}\kappa^{-5/3}\left[\frac{\kappa L}{\sqrt{(\kappa L)^2 + C_L}}\right]^{\frac{5}{3}+p_0} exp\left[-\beta\left\{\left[(\kappa\eta)^4 + C_\eta^4\right]^{1/4} - C_\eta\right\}\right] \quad (17)$$

where η is the Kolmogorov micro-scale and L is the integral scale, characterising the large eddy size. This model spectrum can well indicate the shape of $E(\kappa)$ including the energy-containing and dissipation subranges of turbulence. The Kolmogorov constant C is normally set

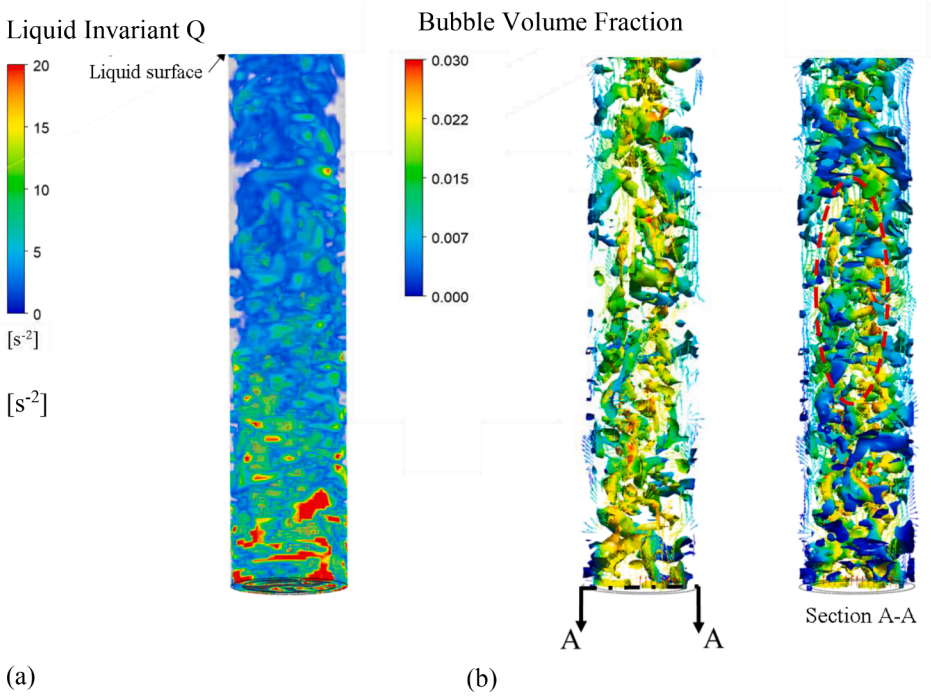

Fig. 16. (a) Volume rendering of liquid phase invariant Q and (b)Iso-surface of liquid phase invariant Q, coloured by corresponding local bubble volume fraction and central cutting plane view.

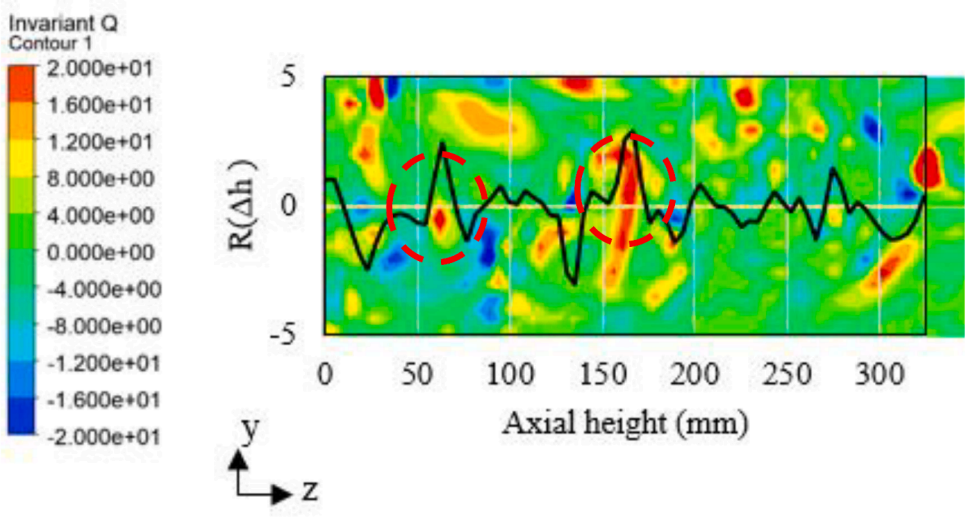

Fig. 17. Spatial correlation coefficient $R(\Delta h)$ along the height of the bubble column from z = 0 mm to z = 325 mm. The background was superimposed with the contours of liquid phase invariant Q.

equal to 1.5 (Pope, 2001) but the value for C was found to be around 1.65 in the present work. The parameter values C_L and C_η are calculated from the integral constraints based on the spectrum obtained by the LES, which satisfy:

$$k = \int_0^\infty E(\kappa)d\kappa \tag{18}$$

and

$$\varepsilon = \int_0^\infty 2\nu\kappa^2 E(\kappa)d\kappa. \tag{19}$$

The parameters β and p_0 are found to be equal to 5.2 and 2.0, respectively. The modified SGS-TDF model gives a $-5/3$ scaling in lower frequency zone while presents a -3 scaling law measured based on the wave number κ larger than the typical wave number characterized by the bubble size, i.e. $\kappa_B = \frac{2p}{d_B} = 1050m^{-1}$. Here, the representative bubble frequency is estimated by $f_b = |\boldsymbol{u}_G - \boldsymbol{u}_L|/2\pi d_B = 13$ Hz using the bubble mean diameter of 2.55 mm [36]. It can be seen from Fig. 15 that the transition for different scaling laws in $E_{11}(\kappa)$ takes place at about $f_1 \approx 15$ Hz, where the left of the transition location shows the $-5/3$ slope while the right side of the transition give rise to the -3 scaling, clearly indicating the feature of feeding of bubble induced turbulence to the turbulent kinetic energy. For the present case, this may indicate that the turbulence due to the bubble wake induced turbulence is fed into the liquid shear turbulence at frequencies around $f_1 \approx 15$ Hz, close to the representative bubble frequency.

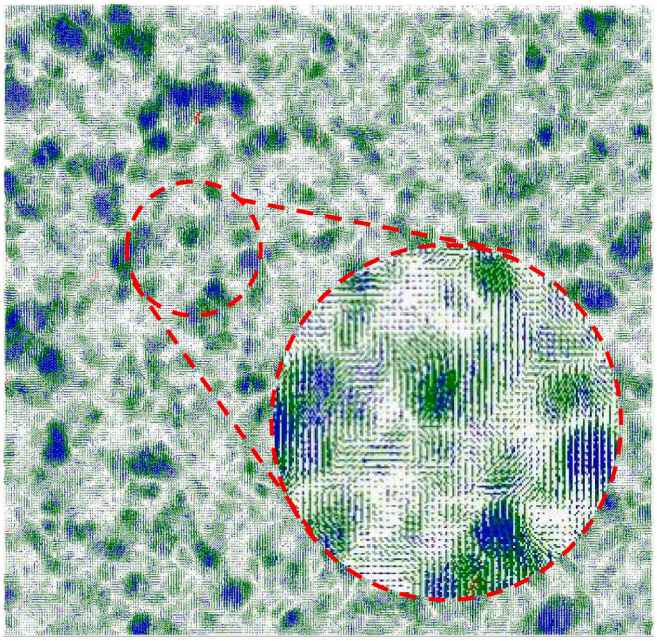

Fig. A1. Instantaneous velocity vector of liquid flow field in bubble column, measured by using the PIV measurement system. (Green: high-quality velocity capture; Blue: insufficient information (no tracer in the region, mostly identified as a bubble occupied in bubbly flow); Red: local error).

In order to describe the effect of the SGS-TDF on turbulent eddy structural behaviour in the bubble column, the vorticity based on *Q*-criterion was assessed. As *Q* represents the local balance between the shear strain rate and vorticity magnitude, defining vortices as the zone where the vorticity magnitude is greater than the magnitude of rate-of-strain, it can be expected that such evaluation would give a qualitative description of the eddy structures existing in the bubble column. The expression for *Q*, which characterises the eddy structure evolution, is defined by $Q = \frac{1}{2}||\overline{\Omega}||^2 - ||\overline{S}||^2$. It is expected that turbulent large eddy structure development in the bubble column would be significantly affected by the entrained bubbles while this interaction between the bubbles and turbulent eddies has been accounted for in the modified SGS model. Thus, a correlation to reflect this coupling can be presented. Fig. 16(a) shows volume rendering of the vorticity indicator *Q* among the bubble column and (b) shows the isosurface of $Q = 20\ s^{-2}$ in the bubble column at $t = 90$ s, coloured by the local bubble volume fraction value. The invariant *Q* can visually represent the distribution of eddies at various scales within the fluid domain. However, some details may not be very distinct in volume rendering. Nevertheless, when restricting the analysis to $Q = 20\ s^{-2}$, the distribution of eddies associated with this value becomes visible. When using the local gas volume fraction rendering, it can be observed that the central region of the bubble column exhibits a higher gas volume fraction. Examining the gas volume fraction distribution within each eddy on a cross-section reveals a clear presence of strongly entrained bubbles within each eddy. Consequently, each eddy's cross-section exhibits a maximum gas volume fraction near the centre, gradually decreasing towards the eddy's periphery. It can be concluded that the bubble volume fraction is strongly coupled with the vorticity indicator *Q*, in particular for the central high bubble volume fraction region. We propose the following spatial correlation between the local bubble volume fraction and *Q* magnitude to characterise the interaction of large turbulent eddies with the entrained bubbles along the axial height of the bubble column, defined by

$$R(\Delta h) = \frac{\overline{\alpha_G^{'}(h_0)|\boldsymbol{Q}^{'}(h_0+\Delta h)|}}{\sqrt{\alpha_G^{'2}(h_0)}\sqrt{|\boldsymbol{Q}^{'2}(h_0)|}} \tag{20}$$

where Eq. (20), $\alpha_G^{'}$ and *Q*' are defined by

$$\alpha_G^{'} = \alpha_G - \frac{1}{h}\int_0^h \alpha_G dz, \tag{21}$$

$$Q^{'} = Q - \frac{1}{h}\int_0^h Q dz. \tag{22}$$

Fig. 17 presents the spatial correlation coefficient $R(\Delta h)$ along the centreline at different axial height from $\Delta h = 0$ to $\Delta h = 0.325$ m with background superposed by the snapshots of the instantaneous *Q* distribution in the cutting plane of the bubble column. It can be seen from the figure that along the centreline, higher values of *Q*, coloured in red, are always accompanied by larger variations in the correlation coefficient $R(\Delta h)$ along the height. This can be interpreted as the consequence of energy containing turbulent large eddy development, which give rise to the local vorticity fluctuation around the spatially averaged shear induced vorticity along the height of the bubble column.

Table A1
Summary on the selective work on turbulent dispersion force (TDF).

Literatures related to TDF	Main Characteristics	Advantages	Disadvantages
[21,4]	TDF is proportional to the volume fraction gradient	Simple and intuitive model	May yield unrealistic results when the dispersed phase velocity is zero
de Bertodano, 1992; [21]	TDF is proportional to the product of volume fraction gradient and TKE	Captures the effect of both bubble volume fraction and liquid turbulence	Requires accurate modelling of both volume fraction gradient and liquid turbulence
Drew, 2001; de Bertodano, 1998	TDF is proportional to the Reynolds stress tensor	Considers the influence of turbulent stresses on bubble dispersion	Relatively complex and computationally expensive
[11]	Random dispersion without tuneable coefficients	Simpler model without the need for tuning coefficients	May lack accuracy and require further validation
Burns et al., 2004	Favre-Averaged Drag (FAD) model: Double-time averaging of drag term in Reynolds momentum equation	Considers local fluctuation and perform well to most of the CFD cases, even CTD is not appropriate	Performance depend on the accuracy of the underlying turbulence modelling, no bubble shape variation included
Lavieville et al., 2017	Generalized turbulent dispersion (GTD) model: Considers influence of liquid turbulence on drag force	Considers additional terms resulting from statistical average of drag and mass coefficients	Based on RANS modelling approach, local fluctuation information is lost
[43]	Sub-grid-scale turbulent dispersion force model: Incorporates SGS turbulent kinetic energy in dispersion model	Suitable for Large Eddy Simulation (LES) and accounts for SGS turbulence effects	Requires LES approach and accurate modeling of SGS turbulent kinetic energy
[41,31]	Accounts for bubble oscillations and tumbling motion in LES Eulerian-Lagrangian modelling	Includes bubble motion equation with various forces contributing to bubble dynamics	Involves complex modelling and implementation of forces (high computational cost), only applicable for low void-fraction system

4. Conclusions

Euler/Euler Large Eddy Simulations of bubble column bubbly flow have been conducted by considering bubble induced turbulence SGS turbulent dispersion. $\frac{\overline{\alpha_k' u_k'}}{\alpha_k}$ has been included to reflect the filtered eddy fluctuation induced turbulent dispersion, and its potential impact on the dynamic interactions between bubble and surrounding eddies, $(C_s\Delta)^2|S|\left(1+C_b\alpha_G\frac{\Delta}{d_B}\left(\frac{1}{1+St_{SGS}}\right)^{\frac{3}{2}}\right)$, has been implemented. The transient turbulent bubbly flow velocities, transient local volume fraction and bubble fluctuations were captured. The time-averaged velocity profiles of both liquid and gas phases obtained from LES with bubble induced turbulence SGS model were compared with the experimental data and non-modified SGS model simulations. Analysis of the liquid phase turbulent kinetic energy spectrum at different locations on the centreline of the bubble column was presented. The main conclusions are summarised as follows:

1) The consistency of the predicted axial bubble velocity profiles with the experimental data by using the adjusted BSD at the inlet has implied that bubble transportation cannot be well captured by only using a mono size bubble diameter. Bubble dynamics in the bubble column may be still captured by using the adequate SGS-TDF model implemented into Eulerian-Eulerian LES modelling, when mimicking the bubble dynamic motion in sub-grid scale. It has been demonstrated clearly that when using Euler/Euler large-eddy simulations (LES) modelling together with considering the effect of bubble-eddy interaction on SGS turbulent dispersion model, the improvement on the prediction of bubble dynamics was achieved. This implies that the modified SGS turbulent dispersion model plays an equivalent role in revealing the bubble fluctuating motion predicted by using Euler/Lagrange LES modelling approach but with the stochastic dispersion model [41].
2) The cross-sectionally averaged absolute ratio of SGS-TDF force to the time-averaged drag force along the height of the bubble column is around 5 %-10 % with the higher percentage taking place in the lower part of the column. This indicates that the bubble dispersion, especially for bubble lateral dispersion can be remarkably affected by the SGS turbulence. The SGS-TDF plays an important role in radial redistribution of bubble volume fraction profiles while the time-averaged drag force mainly determines the bubble dispersion in the main flow direction.
3) The turbulent kinetic energy spectrum obtained from the Euler/Euler LES modelling for the axial liquid velocity at the given locations by using the modified SGS-TDF model has shown that the turbulent kinetic energy spectrum is still consistent with the trend predicted using the model spectrum as proposed by Pope (2001). This can be attributed to the fact that the bubbly flow in the bubble column has lower bubble volume fraction. For the wavenumber of the turbulent eddies smaller than the characteristic wavenumber based on the bubble size, a $-5/3$ scaling law is observed, while a -3-scaling law can be observed for the wavenumber being larger than the characteristic wavenumber. This clearly demonstrates that the turbulent eddies with the equivalent length scale to the bubbles or smaller ones have a strong impact on the bubble induced turbulence as can be seen from the turbulent kinetic energy spectrum. The transition location for the slopes to change from $-5/3$ to -3 in the turbulent kinetic spectrum occurs at f = 15 Hz when using the modified SGS turbulent dispersion model in LES modelling for the cases in the present study, which is close to the characteristic frequency of bubble rising-up $f_B = 13$ Hz.
4) A correlation between vorticity indicator Q and the local bubble volume fraction is proposed, revealing how the bubble dispersion is affected by the surrounding turbulent eddies.

Declaration of Competing Interest

The authors declare that they have no known competing financial interests or personal relationships that could have appeared to influence the work reported in this paper.

Data availability

Data will be made available on request.

Acknowledgements

This work was financially supported by the National Natural Science Foundation of China (Grant Nos. 21761132026, 91534118).

APPENDIX -i

Applying the filtering operation to the phase-weighted microscopic conservation equation, the filtering form of the governing equations are given by

$$\frac{\partial}{\partial t}(\rho_k\alpha_k)+\nabla\bullet(\alpha_k\rho_k\boldsymbol{u}_k)=0 \tag{A1}$$

$$\frac{\partial}{\partial t}(\alpha_k\rho_k\boldsymbol{u}_k)+\nabla\bullet(\alpha_k\rho_k\boldsymbol{u}_k\boldsymbol{u}_k)=-\nabla\bullet(\alpha_k\tau_k)-\alpha_k\nabla p+\alpha_k\rho_k g+\boldsymbol{M}_{F,k}. \tag{A2}$$

In Eqs. (A1) and (A2), α_k is the filtered void fraction of phase k, defined by averaging the phase-indicator function [14]. k signifies the component, liquid or bubbles with $k = G$ for gas phase and $k = L$ for liquid. $\boldsymbol{u}_k$ is the filtered velocity. The terms on the right-hand side of Eq. (A2) respectively represent the stress, the pressure gradient, gravity and the filtered interphase momentum exchange, which arises from the actions of the interface forces. The residual stress term is expressed as Eq. (A3), given by

$$\tau_k=-\mu_{eff}\left(\nabla\boldsymbol{u}_k+(\nabla\mathbf{u}_k)^T-\frac{2}{3}I(\nabla\bullet\boldsymbol{u}_k)\right) \tag{A3}$$

where μ_{eff} is the effective viscosity of the liquid phase, which may be assumed to be composed of three contributions; the molecular viscosity, the turbulent eddy viscosity and an extra term to model bubble induced turbulence as shown by Eq. (A4),

$$\mu_{eff}=\mu_{L,L}+\mu_{T,L}+\mu_{BI,L}. \tag{A4}$$

The extra viscosity caused by the bubble induced turbulence is now usually modelled based on Sato's model, which is given by

$$\mu_{BI,L} = \rho_L C_{\mu,BI} \alpha_G d_B |\boldsymbol{u}_G - \boldsymbol{u}_L|. \quad \text{(A5)}$$

However, as will be discussed in the present work, this viscosity due to the bubble induced turbulence may also be contributed by the relative fluctuation differences between the bubbles and those turbulent eddies that have equivalent or slightly larger length scale and entrapped the bubbles [25].

APPENDIX-II

Table A1.

References

[1] S. Antal, R. lahey jr, J. Flaherty, Analysis of phase distribution in fully developed laminar bubbly two-phase flow, Int. J. Multiph. Flow 17 (1991) 635–652.
[2] M. Bhole, J. Joshi, D. Ramkrishna, CFD simulation of bubble columns incorporating population balance modeling, Chem. Eng. Sci. 63 (2008) 2267–2282.
[4] P. Carrica, D. Drew, F. Bonetto, R. Lahey jr, A polydisperse model for bubbly two-phase flow around a surface ship, Int. J. Multiph. Flow 25 (1999) 257–305.
[5] P. Chen, M. Duduković, J. Sanyal, Three dimensional simulation of bubble column flows with bubble coalescence and breakup, AIChE J 51 (2005) 696–712.
[6] D. Darmana, R. Henket, N. Deen, J. Kuipers, Detailed modelling of hydrodynamics, mass transfer and chemical reactions in a bubble column using a discrete bubble model: chemisorption of CO2 into NaOH solution, numerical and experimental study, Chem. Eng. Sci. 62 (2007) 2556–2575.
[10] N.G. Deen, T. Solberg, B.H. Hjertager, Large eddy simulation of the gas–liquid flow in a square cross-sectioned bubble column, Chem. Eng. Sci. 56 (2001) 6341–6349.
[11] M. Dhotre, B. Smith, B. Niceno, CFD simulation of bubbly flows: random dispersion model, Chem. Eng. Sci. 62 (2007) 7140–7150.
[13] D.A. Drew, A Turbulent Dispersion Model for Particles or Bubbles. In Analysis and Simulation of Multifield Problems, Springer, Berlin, Heidelberg, 2003, pp. 3–12.
[14] D.A. Drew, S.L. Passman, Theory of Multicomponent Fluids, Vol. 135, Springer Science & Business Media, 2006.
[15] A. Gosman, C. Lekakou, S. Politis, R. Issa, M. Looney, Multidimensional modeling of turbulent two-phase flows in stirred vessels, AIChE J 38 (1992) 1946–1956.
[16] S. Hosokawa, A. Tomiyama, S. Misaki, T. Hamada, Lateral migration of single bubbles due to the presence of wall, Fluids Eng. Division Summer Meeting (2002) 855–860.
[17] Z. Huang, D.D. McClure, G.W. Barton, D.F. Fletcher, J.M. Kavanagh, Assessment of the impact of bubble size modelling in CFD simulations of alternative bubble column configurations operating in the heterogeneous regime, Chem. Eng. Sci. 186 (2018) 88–101.
[18] J. Hunt, T. Auton, K. Sene, N. Thomas, R. Kowe, ICHMT International seminar on transient phenomena in multiphase flow, Yugoslavia, Dubrovnik, 1987, pp. 103–125.
[19] F. Kerdouss, A. Bannari, P. Proulx, CFD modeling of gas dispersion and bubble size in a double turbine stirred tank, Chem. Eng. Sci. 61 (2006) 3313–3322.
[20] A.A. Kulkarni, J.B. Joshi, D. Ramkrishna, Determination of bubble size distributions in bubble columns using LDA, AIChE J 50 (2004) 3068–3084.
[21] R. Lahey jr, M.L. de bertodano, O. jones jr, Phase distribution in complex geometry conduits, Nucl. Eng. Des. 141 (1993) 177–201.
[22] S. Laín, C. Grillo, Comparison of turbulent particle dispersion models in turbulent shear flows, Braz. J. Chem. Eng. 24 (2007) 351–363.
[23] J. Laviéville, N. Mérigoux, M. Guingo, C. Baudry, S. Mimouni, A generalized turbulent dispersion model for bubbly flow numerical simulation in NEPTUNE_CFD, Nucl. Eng. Des. 312 (2017) 284–293.
[25] S. Long, J. Yang, X. Huang, G. Li, W. Shi, M. Sommerfeld, X. Yang, Large-eddy simulation of gas–liquid two-phase flow in a bubble column reactor using a modified sub-grid scale model with the consideration of bubble-eddy interaction, Int. J. Heat Mass Transf. 161 (2020), 120240.
[26] N. Lubchenko, B. Magolan, R. Sugrue, E. Baglietto, A more fundamental wall lubrication force from turbulent dispersion regularization for multiphase CFD applications, Int. J. Multiph. Flow 98 (2018) 36–44.
[27] D. Lucas, E. Krepper, H.-M. Prasser, Prediction of radial gas profiles in vertical pipe flow on the basis of bubble size distribution, Int. J. Therm. Sci. 40 (2001) 217–225.
[29] F. Moraga, A. Larreteguy, D. Drew, R. Lahey jr, Assessment of turbulent dispersion models for bubbly flows in the low Stokes number limit, Int. J. Multiph. Flow 29 (2003) 655–673.
[30] R.F. Mudde, O. Simonin, Two-and three-dimensional simulations of a bubble plume using a two-fluid model, Chem. Eng. Sci. 54 (1999) 5061–5069.
[31] M. Muniz, M. Sommerfeld, On the force competition in bubble columns: a numerical study, Int. J. Multiph. Flow 128 (2020), 103256.
[32] D. Pfleger, S. Gomes, N. Gilbert, H.-G. Wagner, Hydrodynamic simulations of laboratory scale bubble columns fundamental studies of the Eulerian-Eulerian modelling approach, Chem. Eng. Sci. 54 (1999) 5091–5099.
[33] M. Polli, M. di Stanislao, R. Bagatin, E.A. Bakr, M. Masi, Bubble size distribution in the sparger region of bubble columns, Chem. Eng. Sci. 57 (2002) 197–205.
[35] M. Pourtousi, P. Ganesan, J. Sahu, Effect of bubble diameter size on prediction of flow pattern in Euler-Euler simulation of homogeneous bubble column regime, Measurement 76 (2015) 255–270.
[36] V.N. Prakash, J.M. Mercado, L. van Wijngaarden, E. Mancilla, Y. Tagawa, D. Lohse, C. Sun, Energy spectra in turbulent bubbly flows, J. Fluid Mech. 791 (2016) 174–190.
[37] R. Rzehak, E. Krepper, C. Lifante, Comparative study of wall-force models for the simulation of bubbly flows, Nucl. Eng. Des. 253 (2012) 41–49.
[38] W. Shi, N. Yang, X. Yang, A kinetic inlet model for CFD simulation of large-scale bubble columns, Chem. Eng. Sci. 158 (2017) 108–116.
[39] A. Sokolichin, G. Eigenberger, A. Lapin, Simulation of buoyancy driven bubbly flow: established simplifications and open questions, AIChE J 50 (2004) 24–45.
[41] M. Sommerfeld, M. Muniz, T. Reichardt, On the importance of modelling bubble dynamics for point-mass numerical calculations of bubble columns, J. Chem. Eng. Jpn. 51 (2018) 301–317.
[42] M.V. Tabib, S.A. Roy, J.B. Joshi, CFD simulation of bubble column—an analysis of interphase forces and turbulence models, Chem. Eng. J. 139 (2008) 589–614.
[43] M.V. Tabib, P. Schwarz, Quantifying sub-grid scale (SGS) turbulent dispersion force and its effect using one-equation SGS large eddy simulation (LES) model in a gas–liquid and a liquid–liquid system, Chem. Eng. Sci. 66 (2011) 3071–3086.
[44] S. Thakre, J. Joshi, CFD simulation of bubble column reactors: importance of drag force formulation, Chem. Eng. Sci. 54 (1999) 5055–5060.
[47] N. Yang, Q. Xiao, A mesoscale approach for population balance modeling of bubble size distribution in bubble column reactors, Chem. Eng. Sci. 170 (2017) 241–250.

Further readings

[3] BURNS, A. D., FRANK, T., HAMILL, I. & SHI, J.-M. The Favre averaged drag model for turbulent dispersion in Eulerian multi-phase flows. 5th International Conference on Multiphase Flow (ICMF2004). ICMF, 1-17.
[7] M.A.L. DE Bertodano, Turbulent bubbly two-phase flow in a triangular duct, Rensselaer Polytechnic Institute, 1992. PhD Dissertation.
[8] M.A.L. DE Bertodano, Two fluid model for two-phase turbulent jets, Nucl. Eng. Des. 179 (1998) 65–74.
[9] O. DE Bertodano, R. lahey jr, O. Jones, Turbulent bubbly two-phase flow data in a triangular duct, Nucl. Eng. Des. 146 (1994) 43–52.
[12] D.A. Drew, A turbulent dispersion model for particles or bubbles, J. Eng. Math. 41 (2001) 259–274.
[24] Y. Liao, Update to the MUSIG model in ANSYS CFX for reliable modelling of bubble coalescence and breakup, App. Math. Model. 81 (2020) 506–521.
[28] Milelli, m., A numerical analysis of confined turbulent bubble plumes, ETH Zurich, 2002. PhD Dissertation.
[34] S.B. Pope, Turbulent flows, Cambridge University Press, IOP Publishing, 2001.
[40] M. Sommerfeld, D. Broder, Analysis of hydrodynamics and microstructure in a bubble column by planar shadow image velocimetry, Ind. Eng. Chem. Res. 48 (2009) 330–340.
[45] A. Tomiyama, Effects of Eotvos number and dimensionless liquid volumetric flux on lateral motion of a bubble in a laminar duct flow. 2nd Int, Conf. an Multiphase Flow (1995).
[46] P. Welch, The use of fast Fourier transform for the estimation of power spectra: a method based on time averaging over short, modified periodograms, IEEE Trans. Audio Electroacoust. 15 (1967) 70–73.